We are IntechOpen,
the world's leading publisher of
Open Access books
Built by scientists, for scientists

6,900
Open access books available

186,000
International authors and editors

200M
Downloads

Our authors are among the

154
Countries delivered to

TOP 1%
most cited scientists

12.2%
Contributors from top 500 universities

CLARIVATE ANALYTICS
BOOK CITATION INDEX
INDEXED

WEB OF SCIENCE™

Selection of our books indexed in the Book Citation Index
in Web of Science™ Core Collection (BKCI)

Interested in publishing with us?
Contact book.department@intechopen.com

Numbers displayed above are based on latest data collected.
For more information visit www.intechopen.com

Review on Optical Waveguides

Shankar Kumar Selvaraja and Purnima Sethi

Additional information is available at the end of the chapter

Abstract

Optical devices are necessary to meet the anticipated future requirements for ultrafast and ultrahigh bandwidth communication and computing. All optical information processing can overcome optoelectronic conversions that limit both the speed and bandwidth and are also power consuming. The building block of an optical device/circuit is the optical waveguide, which enables low-loss light propagation and is thereby used to connect components and devices. This chapter reviews optical waveguides and their classification on the basis of geometry (Non-Planar (Slab/Optical Fiber)/Planar (Buried Channel, Strip-Loaded, Wire, Rib, Diffused, Slot, etc.)), refractive index (Step/Gradient Index), mode propagation (Single/Multimode), and material platform (Glass/Polymer/Semiconductor, etc.). A comparative analysis of waveguides realized in different material platforms along with the propagation loss is also presented.

Keywords: optical waveguides, integrated optics, optical devices, optical materials, photonics integrated circuits

1. Introduction

Waveguides are indispensable for communication and computing applications as they are immune to electromagnetic interference and induced cross talk and also counter diffraction. Next-generation high-end information processing (bandwidths >1 Tb/s and speed >10 Gb/s) is immensely challenging using copper-based interconnects. Optical interconnects transmit data through an optical waveguide and offer a potential solution to improve the data transmission [1, 2]. There are predominantly two classes of optical waveguide: those in which "classical optical elements, placed periodically along the direction of propagation of the wave, serve to confine the wave by successive refocusing in the vicinity of the optical axis (laser resonators and multiple lens waveguides); and those in which the guiding mechanism is that of multiple

total internal reflection from interfaces parallel to the optical axis" (fiber optical waveguides, slab waveguides, and resonators) [3].

Historically, high-frequency microwave sources had created a furore on guided wave photonics pioneered by Rayleigh and Sommerfeld. The first theoretical description of mode propagation along a dielectric guide was done by Hondros and Debye in 1910 [3]. The first dielectric waveguide to be examined at optical frequencies was the glass fiber used primarily for fiber optics imaging applications [4].

A waveguide can be defined as any structure (usually cylindrical) used for guiding the flow of electromagnetic wave in a direction parallel to its axis, confining it to a region either within or adjacent to its surfaces. In order to understand the propagation of light in a waveguide, it is imperative to derive the wave equation. The electromagnetic wave equation can be derived from the Maxwell's equation, assuming that we are operating in a source free ($\rho = 0,\ J = 0$), linear (ε and μ are independent of E and H), and an isotropic medium. E and H are the electric and magnetic field amplitudes, respectively, ε is the electric permittivity of the medium, and μ is the magnetic permeability of the medium. The equations are:

$$\nabla \times \overline{E} = -\frac{\partial \overline{B}}{\partial t} \tag{1}$$

$$\nabla \times \overline{H} = \frac{\partial \overline{D}}{\partial t} \tag{2}$$

$$\nabla . \overline{D} = 0 \tag{3}$$

$$\nabla . \overline{B} = 0 \tag{4}$$

Here, B and D are magnetic and electric fluxes, respectively. The wave equation derived from the above expressions is:

$$\nabla^2 \overline{E} - \mu\varepsilon \frac{\partial^2 \overline{E}}{\partial t^2} = -\nabla \left(\overline{E} . \frac{\nabla \varepsilon}{\varepsilon} \right) \tag{5}$$

The right-hand side of Eq. (5) is nonzero when there is a gradient in permittivity of the medium. Guided wave medium has a graded permittivity; however, in most structures, the term is negligible. Thus, the wave equation can be written as:

$$\nabla^2 \overline{E} - \mu\varepsilon \frac{\partial^2 \overline{E}}{\partial t^2} = 0, \nabla^2 \overline{H} - \mu\varepsilon \frac{\partial^2 \overline{H}}{\partial t^2} = 0 \tag{6}$$

for electric and magnetic field amplitudes, respectively.

2. Classification of waveguides

Optical waveguides can be classified according to their geometry, mode structure, refractive index (RI) distribution, and material. A dielectric optical waveguide comprises a longitudinally

extended high-index medium called the *Core*, which is transversely surrounded by a low-index medium, called the *Cladding*. A guided optical wave propagates in the waveguide along the longitudinal direction. The characteristics of a waveguide are determined by the transverse profile of its dielectric constant *(x, y)*, which is independent of the *z* coordinate. For a waveguide made of optically isotropic media, the waveguide can be characterized merely with a single spatially dependent transverse profile of the index of refraction, n*(x, y)*. Broadly, the waveguides can be classified as [5]:

- Planar/2-D waveguides: Optical confinement is only in one transverse direction, the core is sandwiched between cladding layers in only one direction (**Figure 1(a)**). Optical confinement is only in the *x*-direction with index profile *n(x).* They are primarily used for high-power waveguide lasers and amplifiers.

- Non-planar/3-D/channel optical waveguide: Comprises of two-dimensional transverse optical confinement, the core is surrounded by cladding in all transverse directions, and *n(x, y)* is a function of both *x* and *y* coordinates as shown in **Figure 1(b)**. A channel waveguide (with guidance in both directions) has a guiding structure in the form of a stripe with a finite width. Examples: channel waveguides (Section 2.3.II) and circular optical fibers [6].

A waveguide in which the index profile changes abruptly between the core and the cladding is called a step-index waveguide, while one in which the index profile varies gradually is called a graded-index waveguide as shown in **Figure 2**. Recently, hybrid index profile waveguide was shown combining both inverse-step index waveguide and graded index waveguides for high-power amplification of a Gaussian single-mode beam [7].

2.1. Waveguide mode

A waveguide mode is an electromagnetic wave that propagates along a waveguide with a distinct phase velocity, group velocity, cross-sectional intensity distribution, and polarization. Each component of its electric and magnetic field is of the form $f(x, y)e^{i\omega t - ihz}$, where *z* is the axis of the waveguide. Modes are referred to as the "characteristic waves" of the structures because their field vector satisfies the homogenous wave equation in all the media that make up the
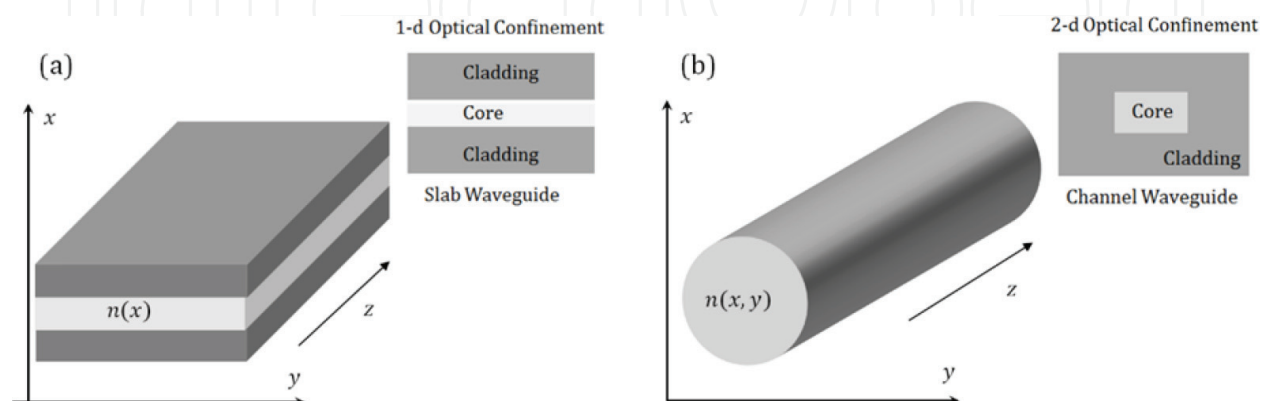
Figure 1. (a) Planar optical waveguide of 1-d transverse *(x)* optical confinement, (b) non-planar optical waveguide of 2-D transverse *(x, y)* optical confinement.
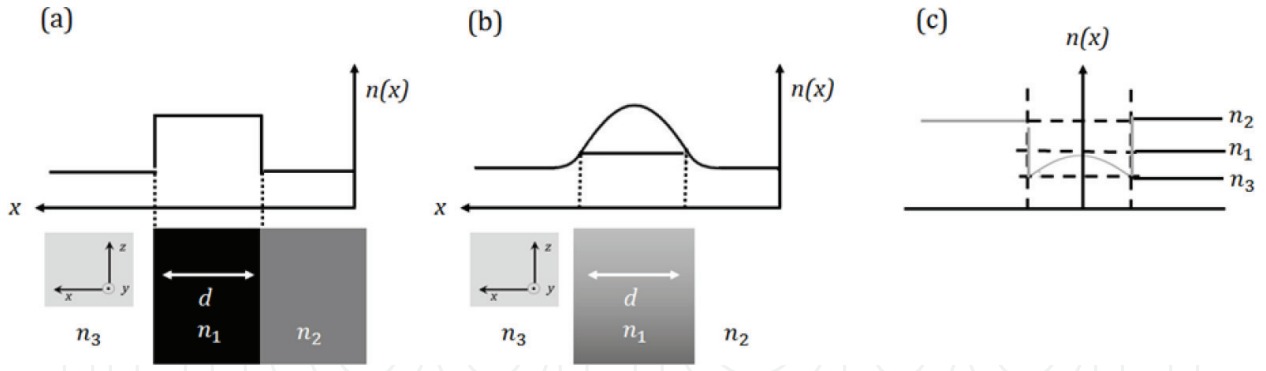
Figure 2. (a) Step-index type waveguide, (b) Graded-index waveguide, and (c) Hybrid waveguide.

guide, as well as the boundary conditions at the interfaces. The electric and magnetic fields of a mode can be written as $E_v(r, t) = E_v(x, y)\exp(i\beta_v z - i\omega t)$ and $H_v(r, t) = H_v(x, y)\exp(i\beta_v z - i\omega t)$, where v is the mode index, $E_v(x, y)$ and $H_v(x, y)$ are the mode field profiles, and β_v is the propagation constant of the mode.

A mode is characterized by an invariant transversal intensity profile and an effective index (n_{eff}). Each mode propagates through the waveguide with a phase velocity of c/n_{eff}, where c denotes the speed of light in vacuum and n_{eff} is the effective refractive index of that mode. It signifies how strongly the optical power is confined to the waveguide core. In order to understand modes intuitively, consider a simple step-index 2-D waveguide and an incident coherent light at an angle θ between the wave normal and the normal to the interface as shown in **Figure 3**. The critical angle at the upper interface is $\theta_c = \sin^{-1}n_c/n_f$ and lower interface $\theta_s = \sin^{-1}n_s/n_f$ and $n_s < n_c$ ($\theta_s < \theta_c$).

Optical modes with an effective index higher than the largest cladding index are (1) **Guided modes** ($\theta_s < \theta < 90°$): As the wave is reflected back and forth between the two interfaces, it interferes with itself. A guided mode can exist only when a transverse resonance condition is satisfied so that the repeatedly reflected wave has constructive interference with itself. Modes with lower index are radiating and the optical power will leak to the cladding regions. They can be categorized as (2) **Substrate radiation modes** ($\theta_c < \theta < \theta_s$): Total reflection occurs only at the upper interface resulting in refraction of the incident wave at the lower interface from either the core or the substrate, (3) **Substrate-cover radiation modes** ($\theta < \theta_c$): No total reflection at either interface. Incident wave is refracted at both interfaces, and it can transversely extend to infinity on both sides of the waveguide, and (4) **Evanescent modes**: Their fields decay exponentially along the z direction. For a lossless waveguide, the energy of an evanescent mode radiates away from the waveguide transversely.

The waveguide dimensions determine which modes can exist. Most waveguides support modes of two independent polarizations, with either the dominant magnetic (quasi-TM) or electric (quasi-TE) field component along the transverse (horizontal) direction. For most applications, it is preferable that the waveguides operate in a single-mode regime for each polarization. This single-mode regime is obtained by reducing the waveguide dimensions until all but
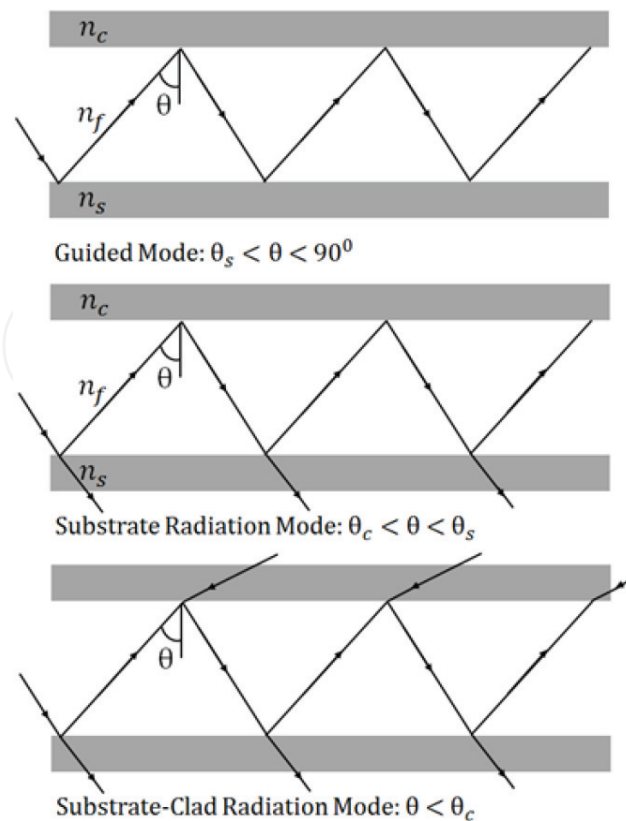
Figure 3. Ray-optical picture of modes propagating in an optical waveguide.

the fundamental waveguide modes become radiating. Fields in the waveguide can be classified based on the characteristics of the longitudinal field components, namely (1) **Transverse electric and magnetic mode** (TEM mode): $E_z = 0$, and $H_z = 0$. Dielectric waveguides do not support TEM modes, (2) **Transverse electric mode** (TE mode): $E_z = 0$ and $H_z \neq 0$, (3) **Transverse magnetic mode** (TM mode): $H_z = 0$ and $E_z \neq 0$, and (4) **Hybrid mode:** $E_z \neq 0$ and $H_z \neq 0$. Hybrid modes exist only in non-planar waveguide.

2.2. Planar waveguide

Homogeneous wave equations exist for planar slab waveguides of any index profile $n(x)$. For a planar waveguide, the modes are either TE or TM.

Infinite slab waveguide: The slab waveguide is a step-index waveguide, comprising a high-index dielectric layer surrounded on either side by lower-index material (**Figure 4**). The slab is infinite in
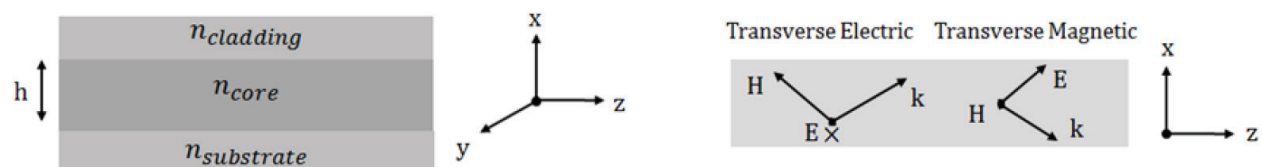
Figure 4. Planar slab waveguide and transverse electric (TE) and transverse magnetic configuration (TM).

the y-z plane and finite in x direction and the refractive index of $n_{core} > n_{cladding}$, $n_{substrate}$ to ensure total internal reflection at the interface. For case (1): $n_{cladding} = n_{substrate}$, the waveguide is denoted as **Symmetric** and for case (2): $n_{cladding} \neq n_{substrate}$, waveguide is **Asymmetric**.

For the electromagnetic analysis of the planar slab waveguide (infinite width), assuming $n_{core} > n_{substrate} > n_{cladding}$, we consider two possible electric field polarizations—TE or TM. The axis of waveguide is oriented in z-direction: k vector of the guided wave will propagate down the z-axis, striking the interfaces and angles greater than critical angle. The field could be TE which has no longitudinal component along z-axis (electric field is transverse to the plane of incidence established by the normal to the interface, and the k vector) or TM depending on the orientation of the electric field.

I. For TE Asymmetric waveguide: E field is polarized along the y-axis, and assuming that waveguide is excited by a source with frequency ω_o and a vacuum wave vector of magnitude $\frac{\omega_o}{c}$, the allowed modes can be evaluated by solving the wave equation in each dielectric region through boundary conditions. For a sinusoidal wave with angular frequency ω_o, the wave equation for the electric field components in each region can be written as ($|k| = \omega\sqrt{\mu\varepsilon} = k$),

$$\nabla^2 E_y + k_0{}^2 n_i{}^2 E_y = 0 \tag{7}$$

here, n_i can be the refractive index of either core, cladding, or the substrate. The solution to Equation (7) can be written as:

$$E_y(x,z) = E_y(x)e^{-j\beta z} \tag{8}$$

due to the translational invariance of the waveguide in z-direction. β is the propagation constant along the z-direction (longitudinal). From Equation (8) and since $\frac{d^2 y}{dx^2} = 0$, we can write:

$$\frac{\partial^2 E_y}{\partial x^2} + \left(k_0{}^2 n_i{}^2 - \beta^2\right)E_y = 0 \tag{9}$$

The solution to the wave equation can be deduced by considering Case (1) $\beta > k_0 n_i$ and E_0 is field amplitude at x = 0, solution is exponentially decaying and can be written as:

$$E_y(x) = E_0 e^{\pm\sqrt{\beta^2 - k_0{}^2 n_i{}^2}x} \tag{10}$$

The attenuation constant $\Upsilon = \sqrt{\beta^2 - k_0{}^2 n_i{}^2}$. Case (2) $\beta < k_0 n_i$, solution has an oscillatory nature and is given by:

$$E_y(x) = E_0 e^{\pm\sqrt{k_0{}^2 n_i{}^2 - \beta^2}x} \tag{11}$$

The transverse wave vector $\kappa = \sqrt{k_0{}^2 n_i{}^2 - \beta^2}$ and the relation between β, κ and k are given by $k^2 = \beta^2 + \kappa^2$.
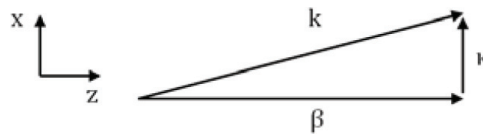
The longitudinal wave vector β (z component of k) must satisfy $k_0 n_{substrate} < \beta < k_0 n_{core}$ ($n_{cladding} \leq n_{core}$) in order to be guided inside the waveguide. Eigen values for the waveguide can be derived using transverse components of electric field amplitudes in three regions as $E_y(x) = Ae^{-\gamma_{cladding}x}$ for $0 < x$; $E_y(x) = B\cos(\kappa_{core}x) + C\sin(\kappa_{core}x)$ for $-h < x < 0$; $\quad E_y(x) = De^{\gamma_{substrate}(x+h)}$ for $x < -h$, where A, B, C, and D are amplitude coefficients to be derived using boundary conditions (E_y, H_z, $\frac{\partial E_y}{\partial x}$ (at $x = 0$) are continuous). Solving the equation, we get $A = B$, $C = -\frac{A\Upsilon_{cladding}}{\kappa_{core}}$, $D = A[\cos(\kappa_{core}h) + \frac{\gamma_{cladding}}{k_{core}}\sin(k_{core}h)]$, and thus:

$$\frac{\partial E_y}{\partial x}\bigg|_{x=-h} = A\left[k_{core}\sin(k_{core}h) - \gamma_{cladding}\cos(k_{core}h)\right](\text{Core})$$

$$= A\left[\cos(k_{core}h) + \frac{\gamma_{cladding}}{k_{core}}\sin(k_{core}h)\right]\gamma_{substrate}(\text{Substrate}).$$

The Eigenvalue equation (**Figure 5(a)**) is given by:

$$\tan(hk_{core}) = \frac{\gamma_{cladding} + \gamma_{subtrate}}{k_{core}\left[1 - \frac{\gamma_{cladding}\gamma_{substrate}}{k_{core}^2}\right]} \tag{12}$$

II. TM Asymmetric waveguide: The field components of the waveguide can be written as:

$H_Y(x,y,t) = H_m(x)e^{-i\omega t}$, $E_x(x,z,t) = \frac{\beta}{\omega\varepsilon}H_m(x)e^{-i(\omega t-\beta z)}$, and $E_z(x,z,t) = \frac{-i}{\omega\varepsilon}$. The Eigen value for β (**Figure 5(b)**) is given by:
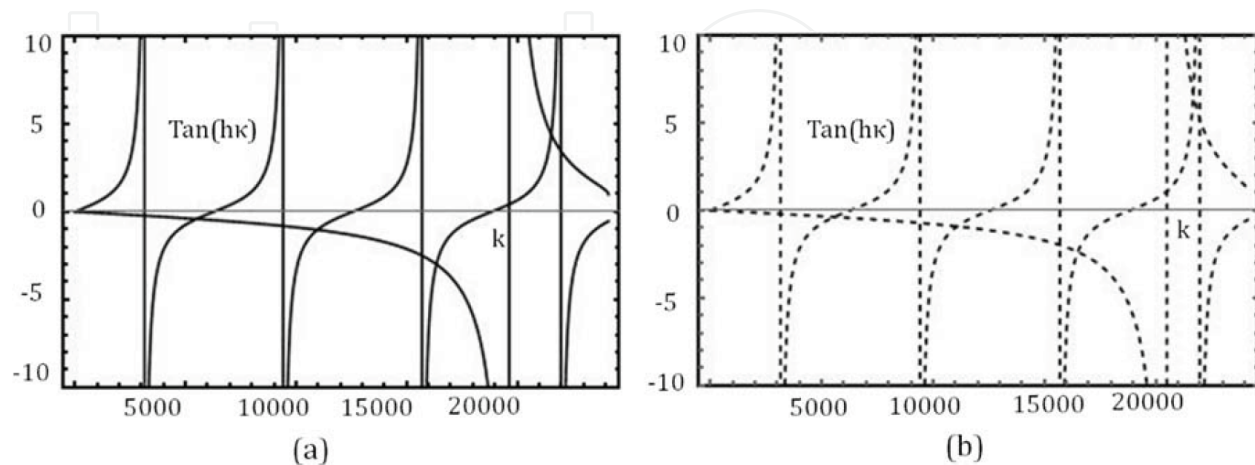
Figure 5. Plot for Eigen value equation for (a) Asymmetric TE mode slab waveguide, (b) Asymmetric TM mode slab Waveguide.

$$\tan(hk_{core}) = \frac{k_{core}\left[\dfrac{n_{core}^2}{n_{substrate}^2}\gamma_{substrate} + \dfrac{n_{core}^2}{n_{cladding}^2}\gamma_{cladding}\right]}{k_{core}^2 - \dfrac{n_{core}^4}{n_{cladding}^2 n_{substrate}^2}\gamma_{cladding}\gamma_{substrate}} \tag{13}$$

III. TE Symmetric waveguide: The field equation of a TE mode within the symmetric waveguide is given by:

$$
\begin{aligned}
E_y &= Ae^{-\gamma\left(x-h/2\right)} && \text{for } x \geq h/2 \\
E_y &= A\frac{\cos\kappa x}{\cos\kappa h/2} \ or \ A\frac{\sin\kappa x}{\sin\kappa h/2} && \text{for } -h/2 \leq x \leq h/2 \\
E_y &= \pm Ae^{\gamma\left(x+h/2\right)} && \text{for } x \leq -h/2
\end{aligned}
\tag{14}
$$

The characteristic Eigen value equation for the TE modes in a symmetric waveguide is given by:

$$
\begin{aligned}
\tan\frac{\kappa h}{2} &= \gamma/k \text{ for even (cos) modes} \\
&= -k/\gamma \text{ for odd (sin) modes}
\end{aligned}
\tag{15}
$$

In order to plot the Eigen values of the TE modes of the symmetric waveguide, solutions of Eq. (15) are plotted for a wavelength of 1.55 μm and different "h" values (15 μm and 3 μm respectively) as shown in **Figure 6**.

The longitudinal wave vector β is quintessential to describe the field amplitudes in all regions of the waveguide. (i) Every Eigen value β corresponds to a distinct confined mode of the system. The amplitude of the mode is established by the power carried in the mode; (ii) only a finite number of modes will be guided depending on the wavelength, index contrast, and
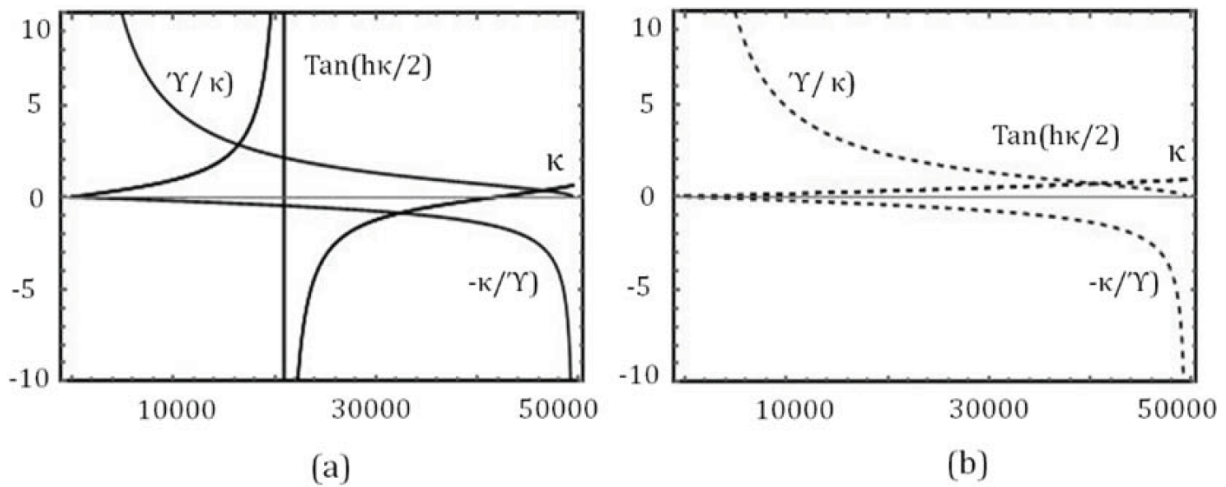
Figure 6. Plot for Eigen value equation for Symmetric TE mode slab waveguide at a wavelength of 1.55 μm for waveguide width of (a) 15 μm and (b) 3 μm. Thick waveguide supports multimode transmission.

waveguide dimensions; (iii) most modes will be unguided, and all modes are orthogonal to each other; (iv) some modes are degenerate. Degenerate modes will share the same value of β but will have distinguishable electric field distributions. The **lower-order mode** is expressed by $\beta_{lowest\ order} \approx kn_{core}$ and **higher-order mode** by $\beta_{lowest\ order} \approx kn_{core} \cos\theta_{critical} \approx kn_{substrate}$. A waveguide is generally characterized by its normalized frequency, given by,

$$V = hk\left(n^2_{core} - n^2_{subtrate}\right)^{1/2}.$$

The approximate number of modes (m) in the waveguide are given by $m \approx V/\pi$. Graphical solution to the waveguide can be evaluated by:

$$V = k_0 h\left(n^2_{core} - n^2_{substrate}\right)^{1/2} \tag{16}$$

$$a = \left(n^2_{substrate} - n^2_{claddding}\right) \Big/ \left(n^2_{core} - n^2_{substrate}\right) \tag{17}$$

$$b = \left(n^2_{eff} - n^2_{substrate}\right) \Big/ \left(n^2_{core} - n^2_{substrate}\right) \tag{18}$$

where a is asymmetry parameter (ranges from 0 (symmetric waveguide) to infinity), b is normalized effective index (ranges from 0 (cutoff) to 1) and $n_{eff} = \beta/k_o$ is the effective index of the waveguide. The normalized dispersion relation is given by (**Figure 7**):

$$V\sqrt{1-b} = v\pi + \tan^{-1}\sqrt{b/(1-b)} + \tan^{-1}\sqrt{(b+a)/(1-b)} \tag{19}$$

where v is an integer. The cut-off condition ($b = 0$) for modes in a step-index waveguide is given by $V = \tan^{-1}\sqrt{a} + v\pi$. The numerical aperture is defined as the maximum angle that an
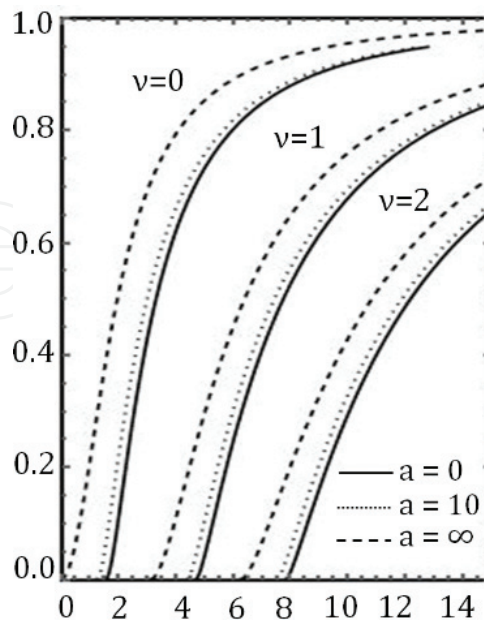
Figure 7. Normalized index b versus normalized frequency V for different values of asymmetry coefficient a (a = 0, a = 10, a = ∞).

incident wave can have and still be guided within the waveguide. It is given by:

$NA = sin\,\theta_{max} = \sqrt{n_{core}^2 - n_{substrate/cladding}^2}$.

IV. TM Symmetric waveguide: The characteristic Eigen value equation for the TM modes in a symmetric waveguide is given by:

$$\tan\frac{\kappa h}{2} = \quad (n_{core}/n_{substrate})^2 \gamma/\kappa : \text{ even (cos) modes}$$

$$= -(n_{core}/n_{substrate})^2 \kappa/\gamma \text{ for odd (sin) modes} \tag{20}$$

Graphical solution to the waveguide can be evaluated using:

$$V = k_0 h \left(n_{core}^2 - n_{substrate}^2\right)^{1/2} \tag{21}$$

$$a = \frac{n_{core}^2 n_{substrate}^2 - n_{cladding}^2}{n_{cladding}^2 n_{core}^2 - n_{substrate}^2} \tag{22}$$

$$b = \left(n_{eff}^2 - n_{substrate}^2\right) / \left(n_{core}^2 - n_{substrate}^2\right) \tag{23}$$

2.3. Non-planar waveguide

The following section describes step-index circular and channel waveguides.

I. Step-index circular waveguide: The wave equation for the step-index circular waveguides in cylindrical coordinates is given by:

$$E(r,\phi,z) = \hat{r}E_r(r,\phi,z) + \hat{\phi}E_\phi(r,\phi,z) + \hat{z}E_z(r,\phi,z) \tag{24}$$

At $z = 0$, field is purely radial (**Figure 8**).The E_z component of the electric field couples only to itself and the scalar wave equation for E_z is given by:

$$\frac{1}{r}\frac{\partial}{\partial r}\left(r\frac{\partial E_z}{\partial r}\right) + \frac{1}{r^2}\frac{\partial^2 E_z}{\partial \phi^2} + \frac{\partial^2 E_z}{\partial z^2} + k_0^2 n^2 E_z = 0 \tag{25}$$

One can write $E_z(r,\phi,z) = R(r)\phi(\varphi)Z(z)$, Eq. (24) can be written as:
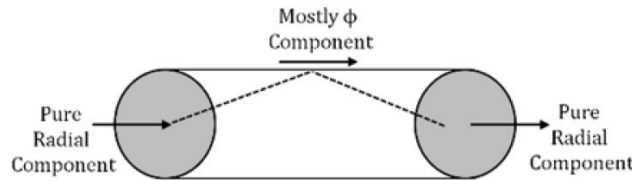
Figure 8. Schematic representation of step-index circular waveguide.

$$R''\Phi Z + \frac{1}{r}R'\Phi Z + \frac{1}{r^2}R\Phi''Z + R\Phi Z'' + k_0^2 n^2 R\Phi Z = 0 \tag{26}$$

The solution to the wave equation is deduced from separation of variables, and we obtain:

$$r^2 \frac{\partial^2 R}{\partial r^2} + r \frac{\partial R}{\partial r} + r^2 \left(k_0^2 n^2 - \beta^2 - \frac{v^2}{r^2} \right) R = 0 \tag{27}$$

The solution is given by Bessel functions: $(1), J_v(\kappa r)$ when $k_0^2 n^2 - \beta^2 - v^2/r^2$ is positive $(\kappa^2 = k_0^2 n^2 - \beta^2)$ and (2) $K_v(\Upsilon r)$ when $k_0^2 n^2 - \beta^2 - v^2/r^2$ is negative $(\gamma^2 = \beta^2 - k_0^2 n^2)$. Bessel function (1) can be approximated by (κr is large) (**Figure 9**):

$$J_v(\kappa r) \approx \sqrt{\frac{2}{\pi \kappa r}} \cos\left(\kappa r - \frac{v}{\pi r} - \frac{\pi}{4} \right) \tag{28}$$

And solution to (2) is

$$K_v(\gamma r) \approx \frac{e^{-\gamma r}}{\sqrt{2\pi \gamma r}} \tag{29}$$

The equation for field distribution in the step-index fiber can be calculated through:

$E_r = \frac{-j\beta}{\kappa^2} \left[A\kappa J'_v(\kappa r) + \frac{j\omega \mu v}{\beta r} B J_v(\kappa r) \right] e^{jv\phi} e^{-j\beta z}$, $\quad E_\phi = \frac{-j\beta}{\kappa^2} \left[\frac{jv}{r} A J_v(\kappa r) - \frac{\omega \mu}{\beta} B\kappa J'_v(\kappa r) \right] e^{jv\phi} e^{-j\beta z}$, $H_r = \frac{-j\beta}{\kappa^2}$ $\left[B\kappa J'_v(\kappa r) - \frac{j\omega \epsilon_{core} v}{\beta r} A J_v(\kappa r) \right] e^{jv\phi} e^{-j\beta z}$ and $H_\phi = \frac{-j\beta}{\kappa^2} \left[\frac{jv}{r} B J_v(\kappa r) - \frac{\omega \epsilon_{core}}{\beta} A\kappa J'_v(\kappa r) \right] e^{jv\phi} e^{-j\beta z}$ for $(r<a)$; a is core's radius. In the cladding $(r>a)$ $E_r = \frac{j\beta}{\gamma^2} \left[C\gamma K'_v(\gamma r) + \frac{j\omega \mu v}{\beta r} D K_v(\gamma r) \right] e^{jv\phi} e^{-j\beta z}$, $E_\phi = \frac{j\beta}{\gamma^2} \left[\frac{jv}{r} C K_v(\gamma r) - \frac{\omega \mu}{\beta} D\gamma K'_v(\gamma r) \right] e^{jv\phi} e^{-j\beta z}$ and $H_r = \frac{j\beta}{\gamma^2} \left[D\gamma K'_v(\gamma r) - \frac{j\omega \epsilon_{clad} v}{\beta r} C K_v(\gamma r) \right] e^{jv\phi} e^{-j\beta z}$.

The V-number or the normalized frequency is used to characterize the waveguide and is defined as:
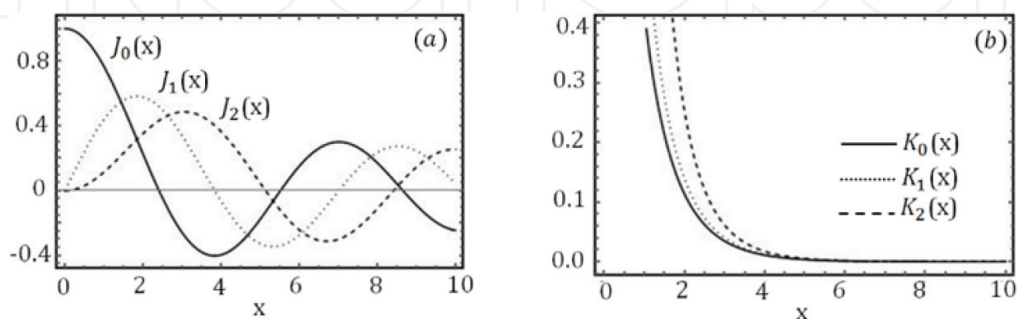
Figure 9. Bessel Function of the (a) first kind (behaves as a damped sine wave) and (b) second kind (monotonic decreasing function).
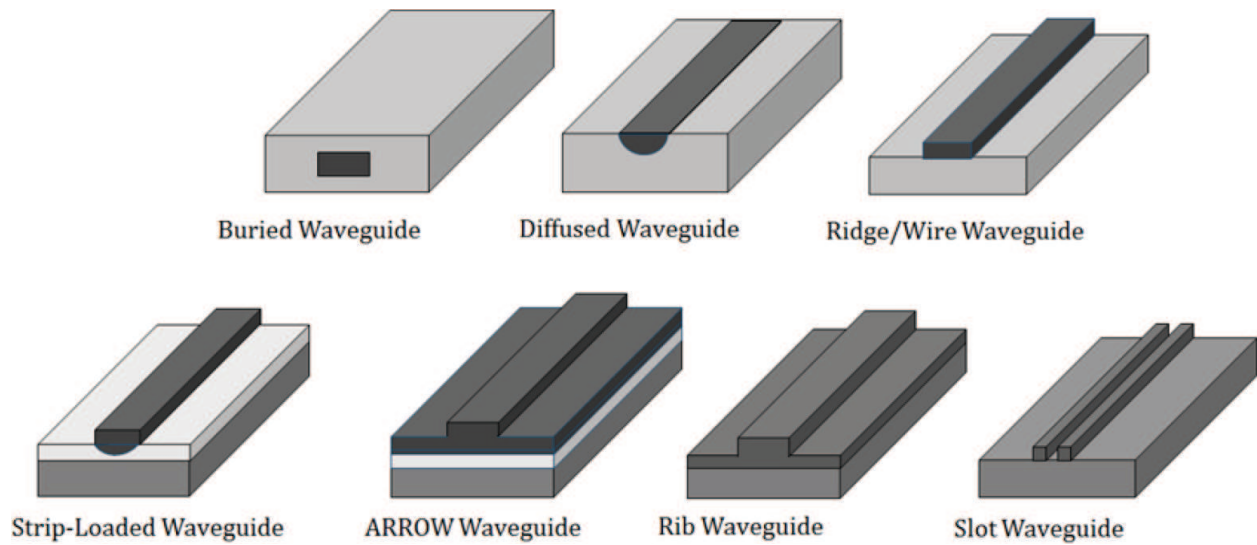
Figure 10. Schematic representation of various channel waveguides.

II. Rectangular dielectric Waveguide: Channel/rectangular waveguides are the most commonly used non-planar waveguides for device applications. Channel waveguides include buried waveguides, strip-loaded, ridge, rib, diffused, slot, ARROW, and so on. **Figure 10** shows the schematic of few of the channel waveguides. The wave equation analysis of a rectangular waveguide can be done by writing the scalar wave equation:

$$\frac{\delta^2 E}{\delta x^2} + \frac{\delta^2 E}{\delta y^2} + \left[k_0^2 n^2(x,y) - \beta^2 \right] E = 0 \tag{30}$$

$$\text{V-number} = a k_0 \sqrt{n_{core}^2 - n_{clad}^2} = \frac{2\pi a}{\lambda} \sqrt{n_{core}^2 - n_{clad}^2} \tag{31}$$

The general representation of the dielectric waveguide along with the electromagnetic field distribution in the regions is shown below:

$\exp(-\gamma_3 x)$ $\exp(-\gamma_5 y)$		$Cos\,(\kappa_y y + \Phi_y)$ $\exp(-\gamma_3 x)$	3	$\exp(-\gamma_3 x)$ $\exp(-\gamma_4(y-b))$	
$Cos\,(\kappa_x x + \Phi_x)$ $\exp(\gamma_5 x)$	5	$Cos\,(\kappa_x x + \Phi_x)$ $Cos\,(\kappa_y y + \Phi_y)$	1	$Cos\,(\kappa_x x + \Phi_x)$ $\exp(-\gamma_4(y-b))$	4
$\exp(-\gamma_2(x-a))$ $\exp(\gamma_5 y)$		$Cos\,(\kappa_y y + \Phi_y)$ $\exp(-\gamma_2(x-a))$	2	$\exp(-\gamma_4(y-b))$ $\exp(-\gamma_2(x-a))$	

where ϕ_x and ϕ_y are phase constants. The characteristic equations are given by $tan\,\kappa_y b = \frac{\kappa_y(\gamma_4+\gamma_5)}{\kappa_y^2-\gamma_4\gamma_5}$ and $tan\,\kappa_x a = n_1^2 \frac{\kappa_x(n_2^2\gamma_3+n_3^2\gamma_2)}{n_2^2 n_3^2 \kappa_x^2 - n_1^2\gamma_2\gamma_3}$ (γ_i) are exponential decay constants. The critical cut-off condition is given by:

$$V = k_0 \frac{a}{2} \sqrt{n_1^2 - n_2^2} \tag{32}$$

The following section describes various types of channel waveguides.

1. Wire waveguide: The schematic of silicon photonic wire waveguide is shown in **Figure 11(a)**. The waveguide consists of a silicon core and silica-based cladding. Since the single-mode condition is very important in constructing functional devices, the core dimension should be determined so that a single-mode condition is fulfilled. The primary requisite is single-mode guiding of the TE_{00} and TM_{00} mode. When the effective refractive index is larger than the cladding and smaller than the core, mode is guided in the waveguide, and guiding will be stronger for higher values of effective index n_{eff}. Thus, modes with effective indices above n_{SiO_2} will not be radiated into the buffer layer and thus will be guided. **Figure 11(b)** depicts the quasi-TE mode of a 220-nm-high and 450-nm-wide silicon waveguide at wavelength of 1.55 μm [8].

Each mode propagates through the waveguide with a phase velocity of c/n_{eff}, where c denotes the speed of light in vacuum and n_{eff} is the effective refractive index felt by that mode. It signifies how strongly the optical power is confined to the waveguide core. Most waveguides support modes of two independent polarizations, with either the major magnetic (quasi-TM) or electric (quasi-TE) field component along the transverse (horizontal) direction.

Figure 11(c) shows n_{eff} as a function of the width of the photonic wire. The n_{eff} depends on the waveguide cross-section, waveguide materials, and the cladding material. Higher-order modes travel with a different propagation constant compared to the lowest-order mode and are less confined in the waveguides. As a consequence of the dissimilar propagation constants, there is modal dispersion which reduces the distance-bandwidth product of the waveguide. Due to the low confinement, first, a large field decay outside the waveguide reduces the maximum density of the devices and, second, in the waveguide bends the higher-order modes
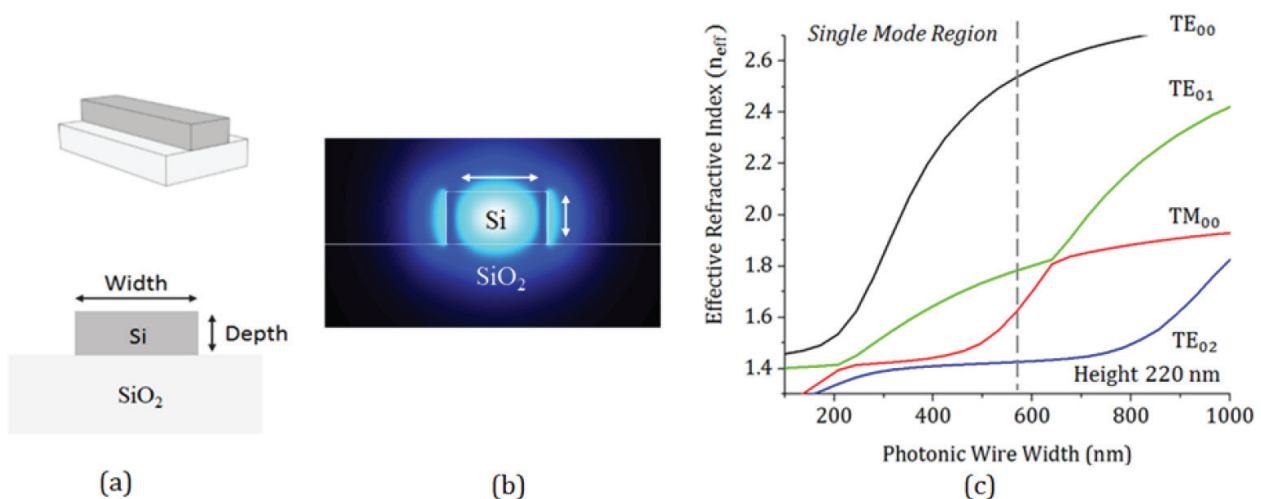
Figure 11. (a) Silicon-on-insulator wire waveguide, (b) quasi-TE mode of a 220-nm-high and 450-nm-wide silicon waveguide at wavelength of 1.55 μm, and (c) effective refractive index (n_{eff}) at 1550 nm for a 220-nm-high silicon photonic wire waveguide. The left of the hashed line is the single-mode region.
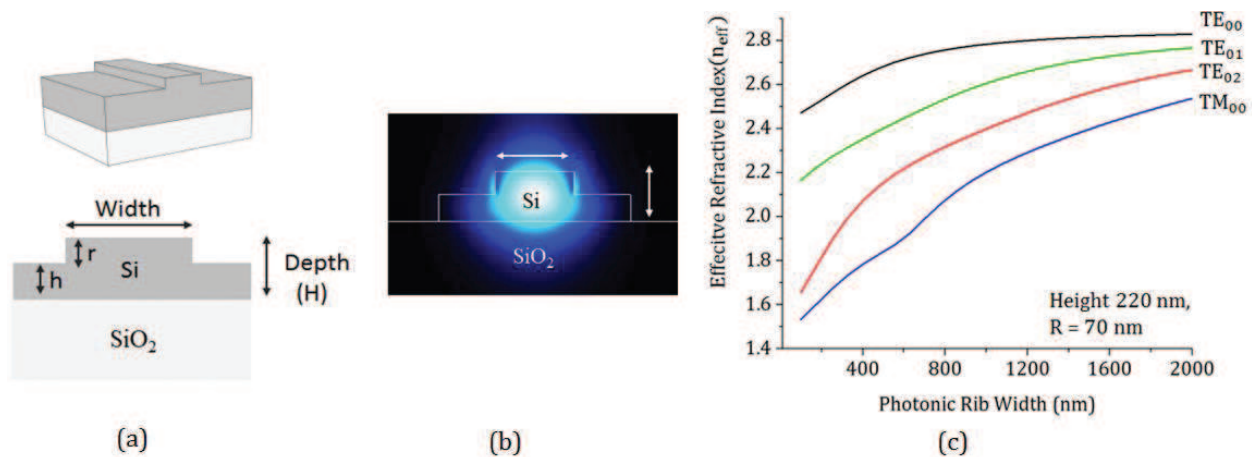
Figure 12. (a) Silicon-on-insulator rib waveguide, (b) quasi-TE mode of a 220-nm-high and 700-nm-wide silicon rib waveguide at wavelength of 1.55 μm, and (c) effective refractive index (n_{eff}) at 1550 nm for 220-nm-high silicon rib waveguide for ridge height (r) = 70 nm.

become leaky resulting in propagation losses. It is desirable that the difference between n_{eff} of the fundamental quasi-TE and quasi-TM modes be large so that the coupling between the modes is limited due to difference in mode profiles and also the phase-mismatch. For widths below ~550 nm, silicon photonic wire will be single mode for each polarization.

2. Rib waveguide: Figure 12(a) and **(b)** shows the schematic and the fundamental quasi-TE mode of a silicon photonic rib waveguide (H = 220 nm, r = 70 nm). Although a rib waveguide can never truly be single mode, by optimizing the design, the power carried by the higher-order modes will eventually leak out of the waveguide over a very short distance, thus leaving only the fundamental mode. **Figure 12(c)** shows the dispersion $\left(n_{eff}\right)$ as a function of the width of the photonic rib waveguide. For widths below ~800 nm, silicon photonic rib waveguide will be single mode for each polarization.
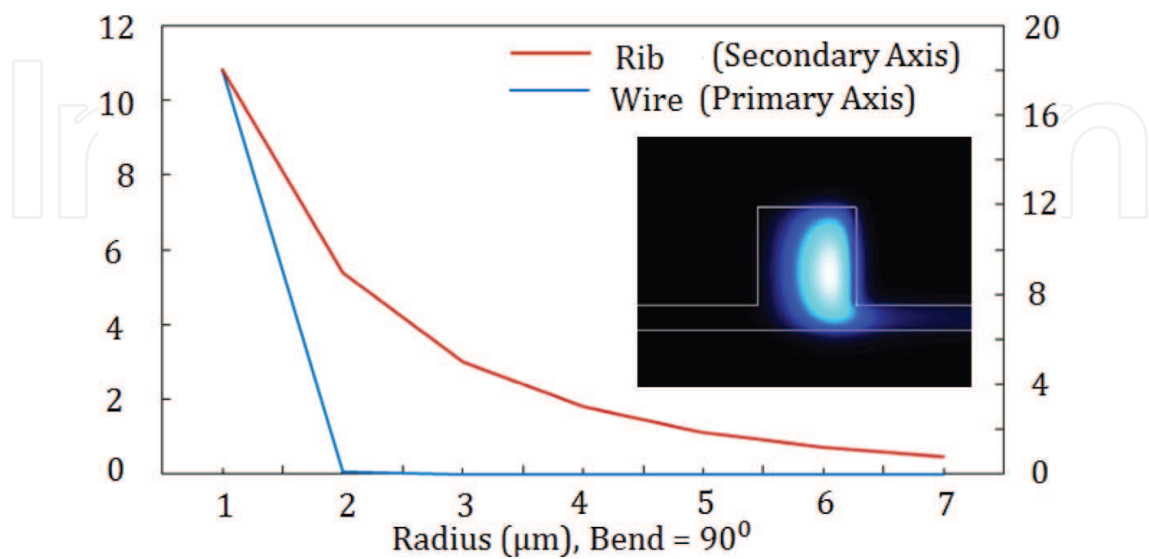
Figure 13. Mode loss for silicon wire (cross-section: 450 × 220 nm^2) and rib (cross-section: 600 × 220 nm^2) waveguides for a 90° bend with increasing bending radii.

Wire waveguides are advantageous as they provide a small bending radius and realization of ultra-dense photonic circuits. However, they have higher propagation losses. On the one hand, wire waveguide allows low-loss sharp bends in the order of a few micrometres, while, on the other hand, the device structures produced are susceptible to geometric fluctuations such as feature drift size (resulting in degradation of device performance) and waveguide sidewall roughness (resulting in propagation losses) [9, 10]. Rib waveguides typically require bend radii >50 μm in SOI to ensure low bend losses, which eventually result in a larger device/circuit footprint. **Figure 13** shows the TE mode loss in silicon wire and rib waveguide for a bend of 90°.

3. Slot waveguide

Slot waveguides are used to confine light in a low-index material between two high-index strip waveguides by varying the gap and dimensions (width and height) of the strip waveguides (**Figure 14(a)**). The normal component of the electric field (quasi TE) undergoes very high discontinuity at the boundary between a high- and a low-index material, which results into higher amplitude in the low-index slot region. The amplitude is proportional to the square of the ratio between the refractive indices of the high-index material (Si, Ge, Si_3N_4) and the low-index slot material (air). On the other hand, the effect of the presence of the slot is minimal on quasi-TM mode, which is continuous at the boundary. When the width of the slot waveguides is comparable to the decay length of the field, electric field remains across the slot and the section has high-field confinement [11–14], which results into propagation of light in the slot section; unlike in a conventional strip waveguide, where the propagating light is confined mainly in the high-index medium.

Figure 14(c) shows the variation in effective index with the waveguide width for different slot gaps. The advantage of a slot waveguide is the high-field confinement in the slot section, which normally cannot be achieved using a simple strip- or a ridge-based waveguide, making it a potential candidate for applications that require light-matter interaction such as sensing [12] and nonlinear photonics [13]. The launching of light into a slot waveguide is normally done by phase matching the propagation constant of the strip waveguide and the slot
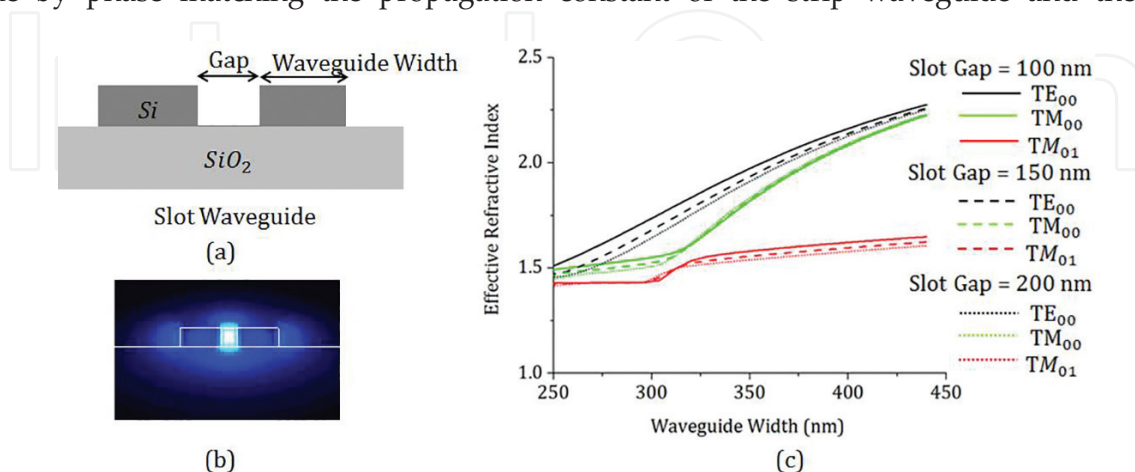

Figure 14. (a) Silicon-on-insulator slot waveguide, (b) Quasi-TE mode of a 220-nm-high (Gap = 100 nm) slot waveguide, (b) variation of effective refractive index with waveguide width for slot gap of 100, 150, and 200 nm, respectively, at a wavelength of 1.55 μm.

waveguide. However, efficient coupling still remains a challenge because of scattering loss and mode mismatch of the slot and strip waveguides, with a reported propagation loss between 2 and 10 dB/cm [14].

4. Strip-loaded waveguide

A strip-loaded waveguide is formed by loading a planar waveguide, which already provides optical confinement in the x direction, with a dielectric strip of index $n_3 < n_1$ or a metal strip to facilitate optical confinement in the y direction, as shown in **Figure 15(a)**. Strip-loaded waveguides do not require half-etching in waveguide fabrication and is therefore easier to fabricate. **Figure 15(a)** shows the schematic of a hydrogenated amorphous silicon strip-loaded waveguide where a thermal oxide is inserted between the layers for passivation [15]. **Figure 15(b)** shows the optical field for the waveguide for a 75-nm-thick and 800-nm-wide strip-loaded waveguide and **Figure 15(c)** depicts the variation in effective index with the strip waveguide width.
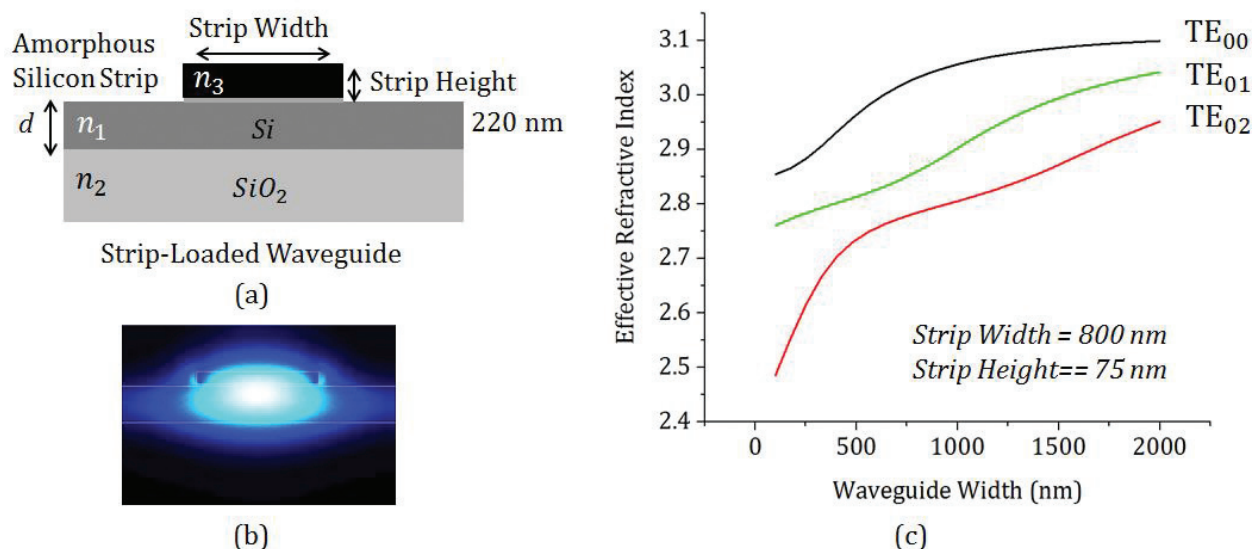
Figure 15. (a) Hydrogenated amorphous strip-loaded waveguide, (b) Quasi-TE mode of a 220-nm-high, 800-nm-wide, 75-nm-thick strip Waveguide, (c) Variation of effective refractive index with strip width at a wavelength of 1.55 μm.

5. Suspended waveguide

Suspended waveguides have enabled new types of integrated optical devices for applications in optomechanics, nonlinear optics, and electro-optics. Fabrication involves removing a sacrificial layer above or below a waveguide core layer to design these waveguides [16]. Increasing absorption loss of SiO_2 at longer wavelengths makes it challenging to utilize SOI for low-loss components in the mid-infrared (MIR) [17]. Removing the SiO_2 layer opens the possibility of extending the low-loss SOI wavelength range up to ~8 μm. For MEMS, it is imperative to have waveguides that can be mechanically actuated. This requires waveguides that are released
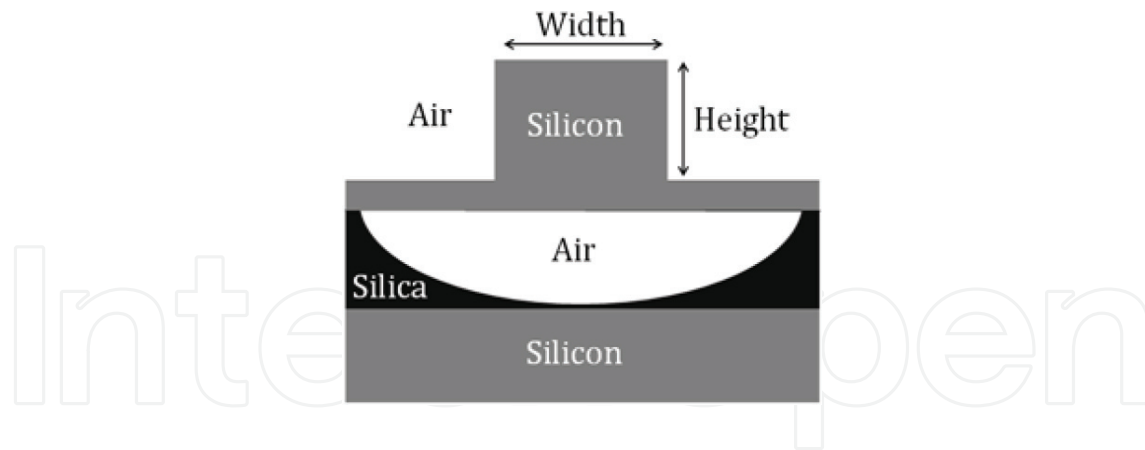
Figure 16. Schematic of a suspended waveguide.

from the substrate, for example, through surface micromachining [17]. **Figure 16** shows the schematic of a suspended waveguide [18].

6. Triplex^{TM} technology

TriPleX waveguides are a family of waveguide geometries that is based on an alternating layer stack consisting of two materials: Si_3N_4 and SiO_2. The waveguide geometries are categorized as box shell, single stripe (propagation loss <0.03 dB/cm), symmetric double stripe (propagation loss <0.1 dB/cm), and asymmetric double stripe (propagation loss <0.1 dB/cm) as shown in **Figure 17(a)** [19]. Different confinement regimes can be optimized
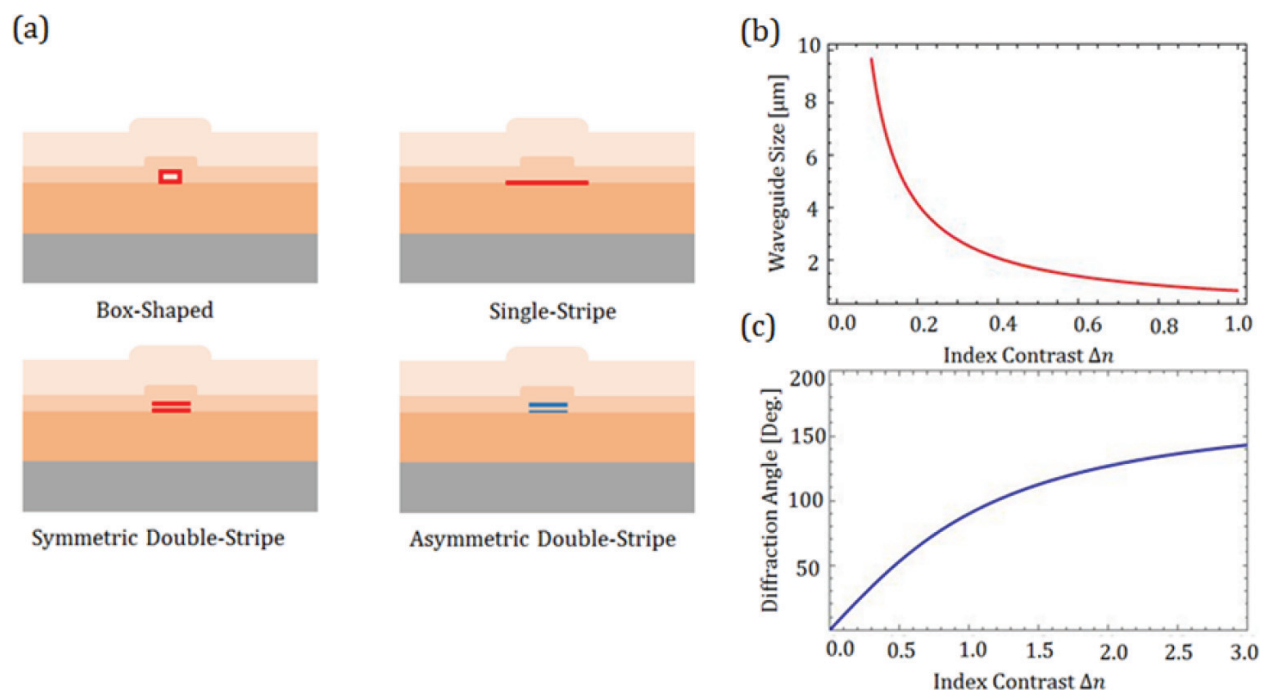
Figure 17. (a) Schematic of different type of TriPleX waveguides, (b) Variation in waveguide size of the box-shaped waveguide, and (c) its diffraction angle versus the index contrast.

for specific applications for these waveguides and tunable birefringence- and polarization dependent loss (PDL) can be achieved. Propagation losses (<0.1 dB/cm), very low PDL (< 0.1 dB/cm), and easy interconnection with optical fibers (<0.15 dB/facet) have been demonstrated in single-mode box-shaped waveguides [20]. Moreover, fabrication of the waveguide is a low-cost and simple process.

LioniX TriPleX technology is a versatile photonics platform suited for applications such as communications, biomedicine, sensing, and so on, over a broadband range of 0.4 to 2.35 μm [21]. **Figure 17(b)** and **(c)** depicts the variation in waveguide size and diffraction angle with index contrast of the box-shaped geometry for a wavelength of 1.55 μm.

7. Photonic crystal waveguide

Photonic crystal waveguides guiding mechanism is different from that of a traditional waveguide, which is based on internal reflection. A photonic crystal is a periodic dielectric structure with a photonic band gap, that is, a frequency range over which there is no propagation of light. The introduction of line defects into a photonic crystal structure creates an optical channel for propagation of light. If the line defect is properly designed, the resulting guiding mode falls within a photonic band gap, is highly confined, and can be used for guiding light. The guiding mode can also be designed to be broadband and thus gives rise to a compact, broadband photonic crystal waveguide [22]. Application of these waveguides includes nanofluidic tuning, RI measurements, optical characterization of molecule orientation, and biosensing.

8. Diffused waveguide

A diffused waveguide is formed by creating a high-index region in a substrate through diffusion of dopants, such as a $LiNbO_3$ waveguide with a core formed by Titanium (Ti) diffusion. Due to the diffusion process, the core boundaries in the substrate are not sharply defined. A diffused waveguide has a thickness defined by the diffusion depth of the dopant and a width defined by the distribution of the dopant. Alternatively, the material can be exchanged with the substrate. Ion-exchanged glass waveguide is fabricated by diffusing mobile ions originally in glass with other ions of different size and polarizability [23].The additional impurities cause a change in refractive index that is approximately proportional to their concentration. A material can also be implanted using an ion implanter within the waveguide. However, this process damages the lattice and is therefore followed by annealing.

9. ARROW waveguide

In anti-resonant reflecting optical (ARROW) waveguides, light confinement is realized by choosing the cladding layer thicknesses accordingly to create an anti-resonant Fabry-Perot reflector

for the transverse component of the wave vector at the desired wavelength. Even though the ARROW mode is leaky, low-loss propagation over large distances can be achieved. Yin *et al.* have designed an ARROW waveguide exhibiting single-mode confinement and low-loss light propagation in a hollow air core on a semiconductor chip [24]. ARROW waveguides with non-solid low-index cores have applications in gas and liquid sensing, quantum computing, quantum communications, and Raman scattering spectroscopy. Chalcogenide rib ARROW structures have also been shown with propagation loss ~6 dB/cm to design opto-chemical sensors in the near- and mid-IR region [25].

10. Augmented waveguide

Light confinement in a low-index media has been shown in ARROW, slot, and plasmonic waveguides. However, ARROW waveguide has low confinement and is thus leaky. Strong light confinement in the low-index medium can be achieved by using silicon slot and plasmonic waveguide. Fabrication of the slot waveguide is cumbersome and hybrid plasmonic waveguide suffers from additional propagation losses due to the presence of metal. Augmented waveguide confines light efficiently in the low-index region by reducing the reflection at the high index-low index interface in a high-index contrast waveguide, which results in enhancement of light confinement in the low-index region [26]. **Figure 18** shows the schematic of an augmented low-index waveguide.

Waveguides can be classified on the basis of different material platforms. Wavelength range, ease of fabrication, compactness, and CMOS compatibility are few of the determining factors when selecting a material for a specific application. **Table 1** compares various waveguide platforms along with their propagation losses [27]. **Figure 19** shows variation of index contrast with footprint for few material platforms.
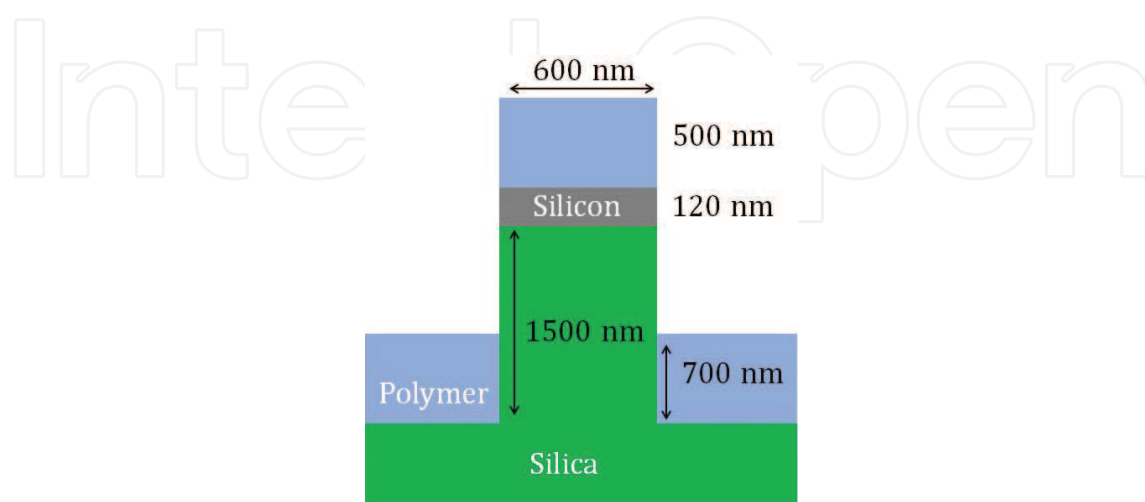
Figure 18. Schematic of an augmented waveguide.

Material platforms	Waveguides	Range	Configuration	Propagation Loss
Semiconductor materials	Silicon	Mid-IR	Silicon nanophotonic waveguide	~4 dB/cm (2030 nm) ~10 dB/cm (2500 nm) [28]
		Mid/Near-IR	Suspended silicon-membrane ridge waveguide (TM mode)	~2.8 ± 0.5 dB/cm (3.39 μm) ~5.6 ± 0.3 dB/cm (1.53 μm) [29]
		Mid/Near-IR	Silicon on porous silicon (SiPSi)	~2.1 ± 0.2 dB/cm (1.55 μm) ~3.9 ± 0.2 dB/cm (3.39 μm) [30]
	Germanium	Mid-IR	Germanium on silicon strip waveguide	~2.5 − 3 dB dB/cm [31] (~5.15-5.4 μm)
		Far-IR	Germanium on silicon strip waveguide	~2.5 dB dB/cm [32] (~5.8 μm)
		Mid-IR	Germanium on silicon rib waveguide	~2.4 ± 0.2 dB/cm [33] (~3.8 μm)
		Mid-IR	Germanium-rich silicon germanium platform-based rib waveguide	1.5 ± 0.5 dB/cm [34] (~4.6 μm)
		Mid IR/Far-IR	Silicon germanium/silicon-based graded index waveguides	~1 dB/cm (4.5 μm) ~2 dB/cm (7.4 μm) [35]
		Mid-IR	Germanium-on-silicon-on-insulator waveguides	3.5 dB/cm (3.682 μm) [36]
		Mid-IR	Silicon germanium ridge waveguide on a silicon substrate	0.5 dB/cm (4.75 μm) [37]
		Far-IR	Germanium on GaAs ridge waveguide	4.2 dB/cm (10 μm) [38]
	Gallium arsenide (GaAS)	Near-IR	GaAS/Al$_{0.3}$ Ga$_{0.7}$As ridge waveguide for manipulation of single-photon and two-photon states	1.6 dB/cm (1.55 μm) [39]
		Near-IR	Suspended GaAs waveguide	0.4 dB/mm (TE) (1.55 μm) and 6 dB/mm (TM) (1.03 μm) [40]
		Near-IR	GaAs-based single-line defect photonic crystal slab waveguide	0.76 dB/mm (1050–1580 nm) [41]
	Indium phosphide (InP)	Near-IR	InP waveguides based on localized Zn-diffusion process (MOVPE) to mitigate passive loss by p-dopants	0.4 dB/cm (1.55 μm) [42]
		Near-IR	Suspended InP dual-waveguide structures for MEMS-actuated optical buffering	2.2 dB/cm (1.5–1.6 μm) [43]
	Gallium antimony	Mid-IR	GaSb waveguides based on quasi-phase matching (QPM)	~0.7/1.1 dB/cm [44] ~(2/4 μm)
	Quantum dotes	Near-IR	Polymer waveguides containing infrared-emitting nanocrystal quantum dots (PbSe and InAs)	~5 dB/cm (inclusive of fiber coupling loss) [45] (~1550 nm)
	Doped semiconductor	Vis/Near-IR	Rare-earth-doped GaN (gallium nitride) channel waveguide	~5.4/4.1 dB/cm [46] (~633/1550 nm)

Material platforms	Waveguides	Range	Configuration	Propagation Loss
		Near-IR	Erbium-Doped Phosphate Glass Strip-loaded Waveguide on Silicon	$\sim$4.1 dB/cm [47] ($\sim$1535 nm)
	Semiconductor nanomaterials	Mid-IR	Silicon-on-Sapphire Suspended Nanowire	$\sim$1 $\pm$ 0.3 dB/cm [48] ($\sim$4 μm)
		Vis	Tin-oxide nanoribbons-based subwavelength waveguide	$\sim$10 dB/cm [49] ($\sim$400-550 nm)
		Near-IR	Amorphous silicon nanowire	$\sim$4.5 dB/cm [50] ($\sim$1550 nm)
		Near-IR	InP/benzocyclobutene optical nanowires on a GaAs substrate	$\sim$0.8 dB/mm [51] ($\sim$1550 nm)
Silicon-on-insulator waveguides	Silicon-on-Silica	Near-IR	Silicon-on-silica strip waveguide	$\sim$0.6 dB/cm [52] ($\sim$1550 and 2000 nm)
		Near-IR	Silicon-on-silica rib (70-nm etch depth) waveguide	$\sim$0.1 $-$ 0.2 dB/cm [52] ($\sim$1550 and 2000 nm)
		Mid-IR	Silicon-on-silica rib (70-nm etch depth) waveguide	$\sim$1.5 dB/cm [53] ($\sim$3800 nm)
		Near-IR	Silicon-on-silica slot waveguide	$\sim$2.28 $\pm$ 0.03 dB/cm [54] ($\sim$1064 nm)
		Near-IR	Silicon-on-Silica slot waveguide	$\sim$3.7 dB/cm [55] ($\sim$1550 nm)
		Mid-IR	Suspended silicon waveguide	$\sim$3.1 dB/cm (7.67 μm) [56]
		Near-IR	Silicon-on-silica strip waveguide coated with amorphous (TiO_2)	$\sim$2 $\pm$ 1 dB/cm [57] ($\sim$1550 nm)
	Silicon-on-Sapphire	Mid-IR	Silicon-on-sapphire ridge waveguide	$\sim$4.0 $\pm$ 0.7 dB/cm [58] ($\sim$5.4-5.6 μm)
		Mid-IR	Silicon-on-sapphire ridge waveguide	$\sim$4.3 $\pm$ 0.6 dB/cm [59] ($\sim$4.5 μm)
		Mid-IR	Silicon-on-sapphire slot waveguide	$\sim$11 dB/cm [60] ($\sim$3.4 μm)
		Near/Mid-IR	Silicon-on-sapphire nanowire waveguide	$\sim$0.8 dB/cm [61] ($\sim$1550 nm). $\sim$1.1 $-$ 1.4 dB/cm [61] ($\sim$2080 nm) $\sim$<2 dB/cm [61] ($\sim$5.18 μm)
	Silicon-on-nitride	Mid-IR and Near-IR	Silicon-on-nitride ridge waveguide	$\sim$5.2 $\pm$ 0.6dB/cm [62] ($\sim$3.39 μm)
	Thallium-doped SOI Rib/Indium-doped SOI Rib	Near-IR	Thallium-doped silicon waveguide	$\sim$3 dB/cm [63] ($\sim$1.55 μm)
		Near-IR	Indium-doped silicon waveguide, decrease in absorption coefficient $\sim$16 dB/cm [64] (wavelength $\sim$1.55 μm).	
Glass waveguides	Silica glass	Vis	Laser-written waveguide in fused silica for vertical polarization (VP)/ horizontal polarization (HP) beam	$\sim$0.06/0.1 dB/cm [65] ($\sim$777 nm)
		Mid-IR	3D laser-written silica glass step-index high-contrast (HIC) waveguide	$\sim$1.3 dB/cm^3 [66] ($\sim$3.39 μm)

| Material platforms	Waveguides	Range	Configuration	Propagation Loss
		Near-IR	Graded-index (GRIN) Cladding in HIC glass waveguides	~1.5 dB/cm [67] (~1.55 μm)
		Near-IR	High-index, doped silica glass material (Hydex) waveguides	~0.06 dB/cm [68] (~1.55 μm)
	Silicon oxynitride (SiON)	Near-IR	SiON deposited by inductively coupled PECVD-based waveguides	~0.5 ± 0.05 dB/cm, 1.6 ± 0.2 dB/cm and 0.5 ± 0.06 dB/cm [69] (~1330, 1550 and 1600 nm)
	Ion—exchanged glass	Vis	Ti^+/Na^+ ion-exchanged single-mode waveguides on silicate glass	~9 ± 1 dB/cm [70] (~0.405 μm)
		Near-IR	Alkaline aluminum phosphate glasses for thermal ion-exchanged waveguide	~0.53 dB/cm [71] (~1.534 μm)
	Sol-gel glass	Near-IR	Hybrid organic-inorganic glass sol-gel ridge waveguides	~0.1 dB/cm [72] ~(1.55 μm)
		Vis	Sol-gel derived silicon titania slab waveguides films	~0.2 dB/cm [73] (677 nm)
		Vis	Sol–gel-derived glass-ceramic photorefractive films-based waveguide	~0.5 ± 0.2 dB/cm [74] (~635 nm)
	Tungsten tellurite glass	Near-IR	Optical planar channel waveguide-based on tungsten-tellurite glass fabricated by RF Sputtering	~0.44 dB/cm [75] (~1.53 μm)
	Laser-written	Near-IR	Laser-written waveguide in planar light-wave circuit (PLC) glass doped with Boron and Phosphorous	~0.35 dB/cm [76] (~1.55 μm)
		Vis	Laser-written waveguide in fused silica for vertical polarization (VP)/ horizontal polarization (HP) beam	~0.06/0.1 dB/cm [65] (~777 nm)
		Near-IR	Laser-written ferroelectric crystal in glass waveguide	~2.64 dB/cm [77] (~1530 nm)
		Vis	Femtosecond laser-written double-line waveguides in germanate and tellurite glasses	~2.0 dB/cm [78] (~632 nm)
		Near-IR	Ultrafast laser-written waveguides in flexible As_2S_3 chalcogenide glass tape	<0.15 dB/cm [79] (~1550 nm)
Electro-optic waveguides	Lithium niobate	Near-IR	Lithium niobate on insulator rib waveguide	~0.4 dB/cm [80] (~1.55 μm)
		Near-IR	Lithium niobate ridge waveguide	~0.3 dB/cm(TE) and 0.9 dB/cm (TM) [81] (~1.55 μm)
		Near-IR	Periodically poled lithium niobate waveguide	~<1 dB/cm [82] (~1.55 μm)
		Near-IR	Heterogeneous lithium niobate on silicon nitride waveguide	~< 0.2 ± 0.4 dB/cm [83] (~1.54 μm)

Material platforms	Waveguides	Range	Configuration	Propagation Loss
		Near-IR	Lithium Niobate on Insulator Ridge Waveguide	~1 dB/cm [84] (~1.55 μm)
		Near-IR	Thin film strip-loaded (SiN) lithium niobate waveguide	~5.8 dB/cm (TE) 14dB/cm (TM) [85] (~1.55 μm)
		Near-IR	Thin film strip-loaded (a-Si) lithium niobate waveguide	~42 dB/cm (TE) 20dB/cm (TM) [86] (1.55 μm)
		Near-IR	Thin film lithium niobate ridge waveguide	~0.268 dB/cm (TE) 1.3dB/cm (TM) [87] (~1.55 μm)
	Lithium tantalate	Near-IR	Ga^{3+}-diffused lithium tantalate waveguide	~0.2 dB/cm (TE) 0.4 dB/cm (TM) [88] (~1.55 μm)
	Barium titanate (BTO)	Vis	BTO thin films on MgO-based ridge waveguide	~2 dB/cm (TE) [89] (~633 nm)
		Mid-IR	BTO thin films on Lanthanum Aluminate (LAO) with a-Si ridge waveguide	~4.2 dB/cm [90] (~3.0 μm)
	Electro-optic polymer	Near-IR	Hybrid Electro-Optic Polymer and TiO_2 Slot Waveguide	~5 dB/cm [91] (~1550 nm)
	Liquid crystal	Near-IR	PDMS (poly (dimethyl siloxane))-liquid crystal-based optical waveguide	~8dB/cm [92] (~1550 nm)
		Vis	Liquid-crystal core channel waveguide encapsulated in semicircular grooves with glass substrate	~1.3 dB/cm [93] (~632.8 nm)
		Near-IR	Liquid crystal clad shallow-etched SOI waveguide	~4.5 dB/cm [94] (1570 nm)
Polymer-based	Conventional optical polymers	Vis	PMMA (poly(methyl methacrylate))-based optical waveguide	~0.2 dB/cm [95] (~850 nm)
		Vis/Near-IR	Polyurethane (PU)-based optical waveguide	~0.8 dB/cm [95] (~633 and 1064 nm)
		Vis/Near-IR	Epoxy resin-based optical waveguide	~0.3/0.8 dB/cm [95] (~633/1064 nm)
		Vis	Polymer PMMA-based waveguide using femtosecond laser	~0.3 dB/cm [96] (~638 and 850 mm)
	Novel optical polymers	Vis/Near-IR	Polymeric waveguides (WIR30 photopolymer) with embedded micro-mirror	~0.18 dB/cm [97] (~850 nm)
		Vis/Near-IR	Acrylate-based waveguide pattern using photo exposure/laser ablation	~0.02/0.3 and 0.8 dB/cm [95] (~840/1300 and 1550 nm)
		Vis/Near-IR	Telephotonics-OASIC-based optical waveguide	~< 0.01, 0.03, 0.1 dB/cm [95] (~840/1300/1550 nm)
		Near-IR	Dow chemical perfluorocyclobutane(XU 35121)-based waveguide	~0.25 dB/cm [95] (~1300/1550 nm)

Material platforms	Waveguides	Range	Configuration	Propagation Loss
		Near-IR	Circular-core UV-curable epoxies-based optical waveguide	$\sim$0.79 dB/cm [98] ($\sim$1550 nm)
		Vis/Near-IR	Multi-mode Siloxane-based polymer waveguide, single-mode siloxane-based polymer waveguide	$\sim$0.05 dB/cm [99] ($\sim$850 nm)/ $\sim$0.5/1 dB/cm [99] ($\sim$1.31/ 1.55μm)
	Surface plasmon polariton waveguide	Near-IR	Polymer-Silicones-based long range surface plasmon polariton waveguide (LRSPPW)	$\sim$0.5 $-$ 1 dB/mm [100] ($\sim$1.55 μm)
		Near-IR	Exguide ZPU/LFR-based long range surface plasmon polariton waveguide (LRSPPW)	$\sim$1.72 dB/cm [101] ($\sim$1.55 μm).
Hollow waveguides	Metal/ Dielectric Coated	THz	Gold-coated waveguide using liquid phase chemical deposition process	$\sim$1.98/1.89 dB/cm [102] ($\sim$215/ 513 μm)
		THz	Silver-coated waveguide using liquid phase chemical deposition Process	$\sim$1.77/1.62 dB/cm [102] ($\sim$215/ 513 μm)
		Mid-IR	Cadmium sulfide CdS) and PbS (Lead Sulfide) on Ag (Silver)-coated hollow glass waveguide	$\sim$0.037dB/cm [103] ($\sim$2.94 μm)
		THz	High-refractive index composite photonics band-gap Bragg fiber	$\sim$0.3 dB/cm [104] ($\sim$300 μm)
		THz	Silver/polystyrene-coated hollow glass waveguides	$\sim$1.9 dB/m [105] ($\sim$300 μm)
		Vis/Near-IR	Silver/cyclic olefin hollow glass waveguide	$\sim$0.549/0.095 and 0.298 dB/m [106] ($\sim$808/1064 and 2940 nm)
	Hollow glass	Near-IR	Hollow-core optical waveguide (Si Substrate)	$\sim$1.7 dB/cm [107] ($\sim$1.52-1.62 μm)
		Far-IR	Tapered hollow-air core waveguide	$\sim$1.27 dB/cm [108] ($\sim$6.2 μm)
		Vis	Air-core anti-resonant reflecting Optical Waveguide (ARROW)	$\sim$4 dB/cm [109] ($\sim$820-880 nm)
	Chalcogenide	Near-IR	Chalcogenide waveguides ($Ge_{23}Sb_7S_{70}$) fabricated through CMOS-compatible lift-off process: Strip/rib	2-6 /<0.5 dB/cm [110] ($\sim$1550 nm)
		Mid-IR	Chalcogenide waveguides ($Ge_{11.5}As_{24}Se_{64.5}$)	<1 dB/cm (0.3dB at 2000 cm^{-1}) (1500-4000 cm^{-1}) [111]
		Near-IR	Chalcogenide waveguides $Ge_{23}Sb_7S_{70}$ (chlorine-based plasma etching)	**<0.42 dB/cm^{-1}** (1550 nm) [112]
	Liquid core	Vis	Liquid core/(ethylene glycol) air-cladding waveguide	$\sim$0.14 dB/cm (464-596 nm) [113]

Material platforms	Waveguides	Range	Configuration	Propagation Loss
		Vis	Nano porous solid liquid core Waveguide	~0.6 dB/cm (632.8 nm) [114]
Metamaterial optical waveguides		Mid-IR	Suspended silicon waveguide with lateral cladding (subwavelength grating metamaterial)	~0.82 dB/cm (3.8μm) [115]
Titanium dioxide (TiO$_2$)		Vis/Near-IR	Atomic layer deposition (ALD) TiO$_2$ slab waveguide	~2.0-3.5 dB/cm (633 nm) [116] <1 dB/cm (1530 nm) [65]
		Near-IR	Amorphous TiO$_2$ strip waveguide	~2.4-0.2 dB/cm (1.55μm) [117]
Silicon carbide		Near-IR	PECVD silicon-carbide-silicon oxide horizontal slot waveguide	~23.9 ± 1.2 dB/cm (1.3 μm)-TM mode [118]
Silicon nitride on silica[30]		Vis	Silicon-nitride strip waveguide	~2.25 dB/cm. [119] (~532 nm)
		Vis	Silicon-nitride strip waveguide	~0.51 dB/cm. [120] (~600 nm)
		Vis	Silicon-nitride strip waveguide	~1.30 dB/cm. [119] (~780 nm)
		Near-IR	LPCVD Silicon-nitride strip waveguide	~0.04 dB/cm. [121] (~1550 nm)
		Near-IR	TripleX [TM] LPCVD silicon-nitride planar waveguide	~0.02 dB/cm. [122] (~1550 nm)
		Near-IR	900-nm-thick LPCVD Silicon-nitride strip waveguide	~0.37 dB/cm. [123] (~1550 nm)
		Mid—IR	LPVCD silicon-nitride strip waveguide	~0.60 dB/cm. [124] (~2600 nm)
		Mid-IR	Silicon-rich LPVCD silicon-nitride strip waveguide	~0.16 dB/cm. [125] (~2650 nm)/ 2.10 dB/cm. [126] (~3700 nm)
Tantalum pentoxide (Ta_2O_5)- core/silica-clad/ silicon substrate		Near IR	Planar waveguide	~0.03 dB/cm. [127] (~1550 nm)
Suspended silicon-on-insulator waveguide		Mid-IR	Waveguide with Subwavelength grating	~3.4 dB/cm. [17] (~3.8 μm).
Photonic crystal fibers based waveguides		THz	Semiconductor silicon photonic crystal slab waveguides	~0.1/0.04 dB/cm. [128] (~905.7/ 908 μm).
		THz	3-D printed THz waveguide based on Kagome photonic crystal structure	~0.1/0.04 dB/cm. [129] (~905.7/ 908 μm).
		THZ	Kagome-lattice hollow-core silicon photonic crystal slab-based waveguide	~0.875 dB/cm [129] (~400 μm).

Table 1. Material platforms.
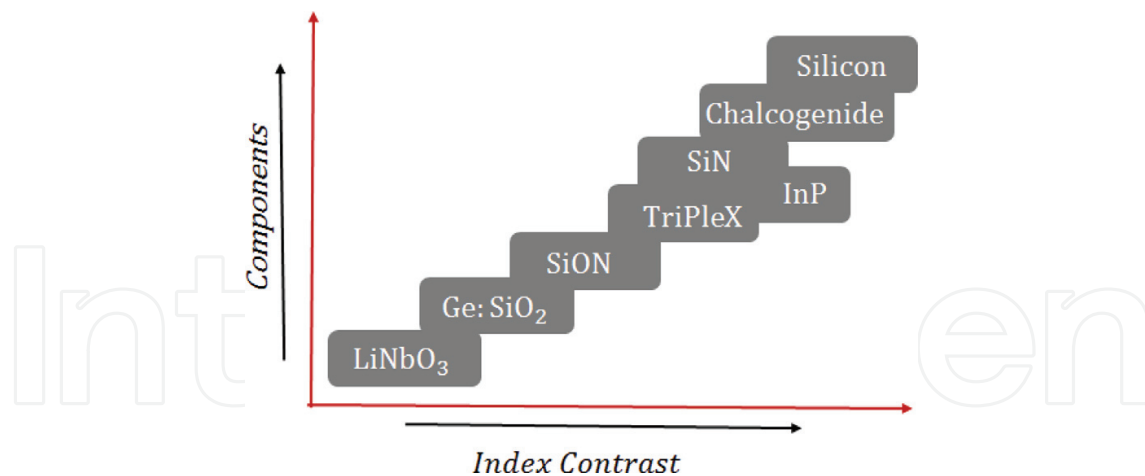
Figure 19. Comparison of different waveguide platforms as a function of index contrast and compactness.

11. Conclusion

Classification of waveguides on the basis of geometry (planar/non-planar), mode propagation (Single/Multi-Mode), refractive index distribution (Step/Gradient Index), and material platform is described briefly. An overview of different kinds of channel waveguides, namely wire, rib, slot, strip-loaded, diffused, TriPleX, suspended, photonic crystal, ARROW, and augmented waveguide is given. A comparative analysis of material platforms used along with their propagation losses and wavelength range is also shown.

Author details

Shankar Kumar Selvaraja* and Purnima Sethi

*Address all correspondence to: shankarks@iisc.ac.in

Centre for Nano Science and Engineering, Indian Institute of Science, Bangalore

References

[1] Hondros D, Debye P. Annals of Physics. 1910;**32**:465

[2] Kapany NS. Fiber Optics Principles and Applications. New York: Academic Press; 1967

[3] Kapany NS, Burke JJ. Optical Waveguides, Quantum Electronics Principles and Applications. New York: Academic Press; 1972

[4] Jia-Ming L. Photonic Devices: Cambridge university text; 2005

[5] Paschotta R. Field Guide to Lasers. Bellingham, WA: SPIE Press; 2008

[6] Pollock CR, Lipson M. Integrated photonics. 2003;**20**(25)

[7] Kim HS, Yoo S. Large mode area inverse index fiber with a graded index profile for high power single mode operation. Optics Express. 2017;**25**(18):21935-21946

[8] Shoji T, Tsuchizawa T, Watanabe T, Yamada K, Morita H. Low loss mode size converter from 0.3 μm square Si wire waveguides to singlemode fibres. Electronics Letters. 2002;**38**(25):1669-1670

[9] Inoue H, Hiruma K, Ishida K, Asai T, Matsumura H. Low loss GaAs optical waveguides. IEEE Transactions on Electron Devices. 1985;**32**(12):2662-2668

[10] Dai D, Tang Y, Bowers JE. Mode conversion in tapered submicron silicon ridge optical waveguides. Optics Express. 2012;**20**(12):13425-13439

[11] Xu Q et al. Experimental demonstration of guiding and confining light in nanometer-size low-refractive-index material. Optics Letters. 2004;**29**(14):1626-1628

[12] Passaro V, La Notte M. Optimizing SOI slot waveguide fabrication tolerances and strip-slot coupling for very efficient optical sensing. Sensors 12.3. 2012:2436-2455

[13] Wang Z, Zhu N, Tang Y, Wosinski L, Dai D, He S. Ultracompact low-loss coupler between strip and slot waveguides. Optics Letters. 2009;**34**(10):1498-1500

[14] Säynätjoki A et al. Low-loss silicon slot waveguides and couplers fabricated with optical lithography and atomic layer deposition. Optics Express. 2011;**19**(27):26275-26282

[15] Maegami Y, Cong G, Ohno M, Okano M, Yamada K. Strip-loaded waveguide-based optical phase shifter for high-efficiency silicon optical modulators. Photonics Research. 2016;**4**(6):222-226

[16] Stievater TH, Pruessner MW, Rabinovich WS, Park D, Mahon R, Kozak DA, Bradley Boos J, Holmstrom SA, Khurgin JB. Suspended photonic waveguide devices. Applied Optics. 2015;**54**(31):F164-F173

[17] Penadés JS, Alonso-Ramos C, Khokhar AZ, Nedeljkovic M, Boodhoo LA, Ortega-Moñux A, Molina-Fernández I, Cheben P, Mashanovich GZ. Suspended SOI waveguide with sub-wavelength grating cladding for mid-infrared. Optics Letters. 2014;**39**(19):5661-5664

[18] Li X, Zhou P, He S, Gao S. Dispersion engineering of suspended silicon photonic wave-guides for broadband mid-infrared wavelength conversion. JOSA B. 2014;**31**(10):2295-2301

[19] Roeloffzen CGH, Hoekman M, Klein EJ, Wevers LS, Timens RB, Marchenko D, Geskus D, et al. Low-loss Si3N4 triPleX optical waveguides: Technology and applications over-view. IEEE Journal of Selected Topics in Quantum Electronics. 2018;**24**(4):1-21

[20] Morichetti F, Melloni A, Martinelli M, Heideman RG, Leinse A, Geuzebroek DH, Borreman A. Box-shaped dielectric waveguides: A new concept in integrated optics? Journal of Lightwave Technology. 2007;**25**(9):2579-2589

[21] Melloni A, Costa R, Cusmai G, Morichetti F. The role of index contrast in dielectric optical waveguides. International Journal of Materials and Product Technology. 2009;**34**(4):421-437

[22] Lin S-Y, Chow E, Johnson SG, Joannopoulos JD. Demonstration of highly efficient waveguiding in a photonic crystal slab at the 1.5-μm wavelength. Optics Letters. 2000; **25**(17):1297-1299

[23] Tervonen A, Honkanen SK, West BR. Ion-exchanged glass waveguide technology: A review. Optical Engineering. 2011;**50**(7):071107

[24] Yin D, Schmidt H, Barber JP, Hawkins AR. Integrated ARROW waveguides with hollow cores. Optics Express. 2004;**12**(12):2710-2715

[25] Balan V, Vigreux C, Pradel A, Llobera A, Dominguez C, Alonso MI, Garriga M. Chalco-genide glass-based rib ARROW waveguide. Journal of Non-Crystalline Solids. 2003;**326**: 455-459

[26] Alam MZ, Sun X, Mo M, Stewart Aitchison J. Augmented low index waveguide for confining light in low index media. Laser & Photonics Reviews. 2017;**11**(3)

[27] Tong XC. Advanced Materials for Integrated Optical Waveguides: Springer; 2016.s

[28] Liu X, Jr RMO, Vlasov YA, Green WMJ. Mid-infrared optical parametric amplifier using silicon nanophotonic waveguides. Nature Photonics. 2010;**4**(8):557

[29] Chiles J, Khan S, Ma J, Fathpour S. High-contrast, all-silicon waveguiding platform for ultra-broadband mid-infrared photonics. Applied Physics Letters. 2013;**103**(15):151106

[30] Mashanovich GZ, Milošević MM, Nedeljkovic M, Owens N, Xiong B, Ee JT, Youfang H. Low loss silicon waveguides for the mid-infrared. Optics Express. 2011;**19**(8):7112-7119

[31] Malik A et al. Germanium-on-silicon mid-infrared arrayed waveguide grating multi-plexers. IEEE Photonics Technology Letters. Sep. 2013;**25**(18):1805-1808

[32] Chang Y-C et al. Low-loss germanium strip waveguides on silicon forthe mid-infrared. Optical Letters. 2012;**37**:2883-2885

[33] Mashanovich GZ, Gardes FY, Thomson DJ, Hu Y, Li K, Nedeljkovic M, Penades JS, Khokhar AZ, Mitchell CJ, Stankovic S, Topley R. Silicon photonic waveguides and devices for near-and mid-IR applications. IEEE Journal of Selected Topics in Quantum Electronics. 2015;**21**(4):407-418

[34] Ramirez JM, Vakarin V, Gilles C, Frigerio J, Ballabio A, Chaisakul P, Le Roux X, et al. Low-loss Ge-rich Si 0.2 Ge 0.8 waveguides for mid-infrared photonics. Optics Letters. 2017;**42**(1):105-108

[35] Brun M, Labeye P, Grand G, Hartmann J-M, Boulila F, Carras M, Nicoletti S. Low loss SiGe graded index waveguides for mid-IR applications. Optics Express. 2014;**22**(1):508-518

[36] Younis U, Lim AE-J, Lo PG-Q, Bettiol AA, Ang K-W. Propagation loss improvement in Ge-on-SOI mid-infrared waveguides using rapid thermal annealing. IEEE Photonics Technology Letters. 2016;**28**(21):2447-2450

[37] Carletti L, Ma P, Yi Y, Luther-Davies B, Hudson D, Monat C, Orobtchouk R, et al. Nonlinear optical response of low loss silicon germanium waveguides in the mid-infrared. Optics Express. 2015;**23**(7):8261-8271

[38] Liao H-Y, Jung S, Chakravarty S, Chen RT, Belkin MA. Low-Loss Ge-on-GaAs platform for mid-infrared photonics. In: Lasers and Electro-Optics (CLEO), 2017 Conference on, pp. 1-2. IEEE. 2017

[39] Wang J, Santamato A, Jiang P, Bonneau D, Engin E, Silverstone JW, Lermer M, et al. Gallium arsenide (GaAs) quantum photonic waveguide circuits. Optics Communications. 2014;**327**:49-55

[40] Stievater TH, Mahon R, Park D, Rabinovich WS, Pruessner MW, Khurgin JB, Richardson CJK. Mid-infrared difference-frequency generation in suspended GaAs waveguides. Optics Letters. 2014;**39**(4):945-948

[41] Sugimoto Y, Tanaka Y, Ikeda N, Nakamura Y, Asakawa K, Inoue K. Low propagation loss of 0.76 dB/mm in GaAs-based single-line-defect two-dimensional photonic crystal slab waveguides up to 1 cm in length. Optics Express. 2004;**12**(6):1090-1096

[42] D'Agostino D, Carnicella G, Ciminelli C, Thijs P, Veldhoven PJ, Ambrosius H, Smit M. Low-loss passive waveguides in a generic InP foundry process via local diffusion of zinc. Optics Express. 2015;**23**(19):25143-25157

[43] Ng WH, Podoliak N, Horak P, Wu J, Liu H, Stewart WJ, Kenyon AJ. Design and fabrication of suspended indium phosphide waveguides for MEMS-actuated optical buffering. IEEE Journal of Selected Topics in Quantum Electronics. 2015;**21**(4):240-246

[44] Roux S, Cerutti L, Tournie E, Gérard B, Patriarche G, Grisard A, Lallier E. Low-loss orientation-patterned GaSb waveguides for mid-infrared parametric conversion. Optical Materials Express. 2017;**7**(8):3011-3016

[45] Olsson YK, Chen G, Rapaport R, Fuchs DT, Sundar VC, Steckel JS, Bawendi MG, Aharoni A, Banin U. Fabrication and optical properties of polymeric waveguides containing nanocrystalline quantum dots. Applied Physics Letters. 2004;**85**(19):4469-4471

[46] Steckl AJ, Heikenfeld JC, Lee D-S, Garter MJ, Baker CC, Wang Y, Jones R. Rare-earth-doped GaN: growth, properties, and fabrication of electroluminescent devices. IEEE Journal of Selected Topics in Quantum Electronics. 2002;**8**(4):749-766

[47] Yan YC, Faber AJD, De Waal H, Kik PG, Polman A. Erbium-doped phosphate glass waveguide on silicon with 4.1 dB/cm gain at 1.535 μm. Applied Physics Letters. 1997;**71**(20):2922-2924

[48] Singh N, Hudson DD, Yi Y, Grillet C, Jackson SD, Casas-Bedoya A, Read A, et al. Midinfrared supercontinuum generation from 2 to 6 μm in a silicon nanowire. Optica. 2015;**2**(9):797-802

[49] Sirbuly DJ, Law M, Yan H, Yang P. Semiconductor nanowires for subwavelength photonics integration. 2005:15190-15213

[50] Grillet C, Carletti L, Monat C, Grosse P, Ben Bakir B, Menezo S, Fedeli JM, Moss DJ. Amorphous silicon nanowires combining high nonlinearity, FOM and optical stability. Optics Express. 2012;**20**(20):22609-22615

[51] Carette M, Vilcot J-P, Bernard D, Decoster D. InP/benzocyclobutene optical nanowires. Electronics Letters. 2008;**44**(15):902-903

[52] Roelkens G. Photonic integration: Beyond telecom and datacom. European Conference Interventional Oncology. 2014. Roelkens, Günther

[53] Nedeljkovic M, Khokhar AZ, Hu Y, Chen X, Soler Penades J, Stankovic S, Chong HMH, et al. Silicon photonic devices and platforms for the mid-infrared. Optical Materials Express. 2013;**3**(9):1205-1214

[54] Li X et al. Experimental demonstration of silicon slot waveguide with low transmission loss at 1064 nm. Optical Communication. 2014;**329**:168-172

[55] Debnath K, Khokhar AZ, Boden SA, Arimoto H, Oo SZ, Chong HMH, Reed GT, Saito S. Low-loss slot waveguides with silicon (111) surfaces realized using anisotropic wet etching. Frontiers in Materials. 2016;**3**:51

[56] Penadés JS, Sanchez-Postigo A, Nedeljkovic M, Ortega-Moñux A, Wangüemert-Pérez JG, Xu Y, Halir R, et al. Suspended silicon waveguides for long-wave infrared wavelengths. Optics Letters. 2018;**43**(4):795-798

[57] Alasaarela T, Korn D, Alloatti L, Säynätjoki A, Tervonen A, Palmer R, Leuthold J, Freude W, Honkanen S. Reduced propagation loss in silicon strip and slot waveguides coated by atomic layer deposition. Optics Express. 2011;**19**(12):11529-11538

[58] Spott A, Yang L, Baehr-Jones T, Ilic R, Hochberg M. Silicon waveguides and ring resonators at 5.5 μ m. Applied Physics Letters. 2010;**97**(21):213501

[59] Baehr-Jones T, Spott A, Ilic R, Spott A, Penkov B, Asher W, Hochberg M. Silicon-on-sapphire integrated waveguides for the mid-infrared. Optics Express. 2010;**18**(12):12127-12135

[60] Zou Y et al. Grating-coupled silicon-on-sapphire integrated slot waveguides operating at mid-infrared wavelengths. Optics Letters. 2014;**39**:3070-3073

[61] Li F, Jackson SD, Grillet C, Magi E, Hudson D, Madden SJ, Moghe Y, et al. Low propagation loss silicon-on-sapphire waveguides for the mid-infrared. Optics Express. 2011; **19**(16):15212-15220

[62] Khan S, Chiles J, Ma J, Fathpour S. Silicon-on-nitride waveguides for mid-and near-infrared integrated photonics. Applied Physics Letters. 2013;**102**(12):121104

[63] Knights AP, Ackert JJ, Logan DF, Huante-Ceron E, Jessop PE. Deep-levels in silicon waveguides: A route to high yield fabrication. Optical and Quantum Electronics. 2012; **44**(12-13):575-580

[64] Logan DF, Velha P, Sorel M, De La Rue RM, Wojcik G, Goebel A, Jessop PE, Knights AP. Charge state switching of deep levels for low-power optical modulation in silicon waveguides. Optics Letters. 2011;**36**(19):3717-3719

[65] Guan J, Liu X, Salter PS, Booth MJ. Hybrid laser written waveguides in fused silica for low loss and polarization independence. Optics Express. 2017;**25**(5):4845-4859

[66] Martínez, Javier, Airán Ródenas, Toney Fernandez, Javier R. Vázquez de Aldana, Robert R. Thomson, Magdalena Aguiló, Ajoy K. Kar, Javier Solis, and Francesc Díaz. "3D laser-written silica glass step-index high-contrast waveguides for the 3.5 μm mid-infrared range." Optics Letters 40, no. 24 (2015): 5818-5821

[67] Hu J, Feng N-N, Carlie N, Petit L, Wang J, Agarwal A, Richardson K, Kimerling L. Low-loss high-index-contrast planar waveguides with graded-index cladding layers. Optics Express. 2007;**15**(22):14566-14572

[68] Duchesne D, Ferrera M, Razzari L, Morandotti R, Little BE, Chu ST, Moss DJ. Efficient self-phase modulation in low loss, high index doped silica glass integrated waveguides. Optics Express. 2009;**17**(3):1865-1870

[69] Rangarajan B, Kovalgin AY, Wörhoff K, Schmitz J. Low-temperature deposition of high-quality silicon oxynitride films for CMOS-integrated optics. Optics Letters. 2013;**38**(6):941-943

[70] Jordan E, Geoffray F, Bouchard A, Ghibaudo E, Broquin J-E. Development of Tl+/Na+ ion-exchanged single-mode waveguides on silicate glass for visible-blue wavelengths applications. Ceramics International. 2015;**41**(6):7996-8001

[71] Wang F, Chen B, Pun EYB, Lin H. Alkaline aluminum phosphate glasses for thermal ion-exchanged optical waveguide. Optical Materials. 2015;**42**:484-490

[72] Najafi SI, Ti T, Sara R, Andrews MP, Fardad MA. Sol-gel glass waveguide and grating on silicon. Journal of Lightwave Technology. 1998;**16**(9):1640

[73] Karasiński P, Tyszkiewicz C, Domanowska A, Michalewicz A, Mazur J. Low loss, long time stable sol–gel derived silica–titania waveguide films. Materials Letters. 2015;**143**:5-7

[74] Lukowiak A, Zur L, Tran TNL, Meneghetti M, Berneschi S, Conti GN, Pelli S, et al. Sol–gel-derived glass-ceramic photorefractive films for photonic structures. Crystals. 2017;**7**(2):61

[75] Gorshkov ON, Grishin IA, Kasatkin AP, Smetanin SV, Churbanov MF, Shushunov AN. Optical planar waveguides based on tungsten-tellurite glass fabricated by rf-sputtering. Journal of Non-Crystalline Solids. 2018;**480**:70-73

[76] Nasu Y, Kohtoku M, Hibino Y. Low-loss waveguides written with a femtosecond laser for flexible interconnection in a planar light-wave circuit. Optics Letters. 2005;**30**(7):723-725

[77] Stone A, Jain H, Dierolf V, Sakakura M, Shimotsuma Y, Miura K, Hirao K, Lapointe J, Kashyap R. Direct laser-writing of ferroelectric single-crystal waveguide architectures in glass for 3D integrated optics. Scientific Reports. 2015;**5**:10391

[78] da Silva, Diego S, Wetter NU, de Rossi W, Samad RE, Kassab LRP. Femtosecond laser-written double line waveguides in germanate and tellurite glasses. In: Laser Applications in Microelectronic and Optoelectronic Manufacturing (LAMOM) XXIII, vol. 10519, p. 105191B. International Society for Optics and Photonics. 2018

[79] Lapointe, Jerome, Yannick Ledemi, Sébastien Loranger, Victor Lambin Iezzi, Elton Soares de Lima Filho, Francois Parent, Steeve Morency, Younes Messaddeq, and Raman Kashyap. "Fabrication of ultrafast laser written low-loss waveguides in flexible As 2 S 3 chalcogenide glass tape Optics Letters 41, no. 2 (2016): 203-206

[80] Krasnokutska I, Tambasco J-LJ, Li X, Peruzzo A. Ultra-low loss photonic circuits in lithium niobate on insulator. Optics Express. 2018;**26**(2):897-904

[81] Hu H, Ricken R, Sohler W, Wehrspohn RB. Lithium niobate ridge waveguides fabricated by wet etching. IEEE Photonics Technology Letters. 2007;**19**(6):417-419

[82] Parameswaran KR, Route RK, Kurz JR, Roussev RV, Fejer MM, Fujimura M. Highly efficient second-harmonic generation in buried waveguides formed by annealed and reverse proton exchange in periodically poled lithium niobate. Optics Letters. 2002;**27**(3):179-181

[83] Chang L, Pfeiffer MHP, Volet N, Zervas M, Peters JD, Manganelli CL, Stanton EJ, Li Y, Kippenberg TJ, Bowers JE. Heterogeneous integration of lithium niobate and silicon nitride waveguides for wafer-scale photonic integrated circuits on silicon. Optics Letters. 2017;**42**(4):803-806

[84] Volk MF, Suntsov S, Rüter CE, Kip D. Low loss ridge waveguides in lithium niobate thin films by optical grade diamond blade dicing. Optics Express. 2016;**24**(2):1386-1391

[85] Li S, Cai L, Wang Y, Jiang Y, Hui H. Waveguides consisting of single-crystal lithium niobate thin film and oxidized titanium stripe. Optics Express. 2015;**23**(19):24212-24219

[86] Wang Y, Chen Z, Cai L, Jiang Y, Zhu H, Hui H. Amorphous silicon-lithium niobate thin film strip-loaded waveguides. Optical Materials Express. 2017;**7**(11):4018-4028

[87] Siew SY, Cheung EJH, Liang H, Bettiol A, Toyoda N, Alshehri B, Dogheche E, Danner AJ. Ultra-low loss ridge waveguides on lithium niobate via argon ion milling and gas clustered ion beam smoothening. Optics Express. 2018;**26**(4):4421-4430

[88] Ren S, Yang X-F, Zhang Z-B, Wong W-H, Yu D-Y, Pun EY-B, Zhang D-L. Crystalline phase, Ga3+ concentration profile, and optical properties of Ga3+-diffused lithium tantalate waveguide. Materials Letters. 2018;**213**:79-83

[89] Petraru A, Siegert M, Schmid M, Schubert J, Buchal C. Ferroelectic BaTiO 3 Thin Film Optical Waveguide Modulators. MRS Online Proceedings Library Archive. 2001;**688**

[90] Jin T, Li L, Zhang B, Lin H-YG, Wang H, Lin PT. Monolithic mid-infrared integrated photonics using silicon-on-epitaxial barium titanate thin films. ACS Applied Materials & Interfaces. 2017;**9**(26):21848-21855

[91] Qiu F, Spring AM, Maeda D, Ozawa M-a, Odoi K, Otomo A, Aoki I, Yokoyama S. A hybrid electro-optic polymer and TiO_2 double-slot waveguide modulator. Scientific Reports. 2015;**5**:8561

[92] d'Alessandro A, Martini L, Civita L, Beccherelli R, Asquini R. Liquid crystal waveguide technologies for a new generation of low-power photonic integrated circuits In: Emerging Liquid Crystal Technologies X, vol. 9384, p. 93840L. International Society for Optics and Photonics. 2015

[93] Wang T-J, Chaung C-K, Li W-J, Chen T-J, Chen B-Y. Electrically tunable liquid-crystal-core optical channel waveguide. Journal of Lightwave Technology. 2013;**31**(22):3570-3574

[94] Ako T, Hope A, Nguyen T, Mitchell A, Bogaerts W, Neyts K, Beeckman J. Electrically tuneable lateral leakage loss in liquid crystal clad shallow-etched silicon waveguides. Optics Express. 2015;**23**(3):2846-2856

[95] Ma H, Jen AK-Y, Dalton LR. Polymer-based optical waveguides: materials, processing, and devices. Advanced Materials. 2002;**14**(19):1339-1365

[96] Pätzold WM, Demircan A, Morgner U. Low-loss curved waveguides in polymers written with a femtosecond laser. Optics Express. 2017;**25**(1):263-270

[97] Dou X, Wang X, Huang H, Lin X, Ding D, Pan DZ, Chen RT. Polymeric waveguides with embedded micro-mirrors formed by metallic hard mold. Optics Express. 2010;**18**(1):378-385

[98] Xu X, Lin M, Jiang S, He Z. Circular-core single-mode polymer waveguide for high-density and high-speed optical interconnects application at 1550 nm. Optics Express. 2017;**25**(21):25689-25696

[99] Dangel R, Hofrichter J, Horst F, Jubin D, La Porta A, Meier N, Soganci IM, Weiss J, Offrein BJ. Polymer waveguides for electro-optical integration in data centers and high-performance computers. Optics Express. 2015;**23**(4):4736-4750

[100] Vernoux C, Chen Y, Markey L, Spârchez C, Arocas J, Felder T, Neitz M, et al. Flexible long-range surface plasmon polariton single-mode waveguide for optical interconnects. Optical Materials Express. 2018;**8**(2):469-484

[101] Kim JT, Park S, Jung Jin J, Park SK, Kim M-S, Lee M-H. Low-loss polymer-based long-range surface plasmon-polariton waveguide. IEEE Photonics Technology Letters. 2007; **19**(18):1374-1376

[102] Doradla P, Giles RH. Dual-frequency characterization of bending loss in hollow flexible terahertz waveguides In Terahertz, RF, Millimeter, and Submillimeter-Wave Technology and Applications VII, vol. 8985, p. 898518. International Society for Optics and Photonics. 2014

[103] Bledt CM, Melzer JE, Harrington JA. Theory and practical considerations of multilayer dielectric thin-film stacks in Ag-coated hollow waveguides. Applied Optics. 2014;**53**(4): A70-A82

[104] Ung B, Dupuis A, Stoeffler K, Dubois C, Skorobogatiy M. High-refractive-index composite materials for terahertz waveguides: trade-off between index contrast and absorption loss. JOSA B. 2011;**28**(4):917-921

[105] Bowden B, Harrington JA, Mitrofanov O. Silver/Polystyrene Coated Hollow Glass Waveguides for the Transmission of THz Radiation. In: Lasers and Electro-Optics, 2007. CLEO 2007. Conference on, pp. 1-2. IEEE. 2007

[106] Melzer JE, Harrington JA. Silver/cyclic olefin copolymer hollow glass waveguides for infrared laser delivery. Applied Optics. 2015;**54**(32):9548-9553

[107] Lo S-S, Wang M-S, Chen C-C. Semiconductor hollow optical waveguides formed by omni-directional reflectors. Optics Express. 2004;**12**(26):6589-6593

[108] Giglio M, Patimisco P, Sampaolo A, Kriesel JM, Tittel FK, Spagnolo V. Low-loss and single-mode tapered hollow-core waveguides optically coupled with interband and quantum cascade lasers. Optical Engineering. 2017;**57**(1). DOI: 011004

[109] Bappi G, Flannery J, Al Maruf R, Bajcsy M. Prospects and limitations of bottom-up fabricated hollow-core waveguides. Optical Materials Express. 2017;**7**(1):148-157

[110] Hu J, Tarasov V, Carlie N, Feng N-N, Petit L, Agarwal A, Richardson K, Kimerling L. Si-CMOS-compatible lift-off fabrication of low-loss planar chalcogenide waveguides. Optics Express. 2007;**15**(19):11798-11807

[111] Ma P, Choi D-Y, Yi Y, Gai X, Yang Z, Debbarma S, Madden S, Luther-Davies B. Low-loss chalcogenide waveguides for chemical sensing in the mid-infrared. Optics Express. 2013;**21**(24):29927-29937

[112] Chiles J, Malinowski M, Rao A, Novak S, Richardson K, Fathpour S. Low-loss, submicron chalcogenide integrated photonics with chlorine plasma etching. Applied Physics Letters. 2015;**106**(11):111110

[113] Lim J-M, Kim S-H, Choi J-H, Yang S-M. Fluorescent liquid-core/air-cladding waveguides towards integrated optofluidic light sources. Lab on a Chip. 2008;**8**(9):1580-1585

[114] Gopalakrishnan N, Sagar KS, Christiansen MB, Vigild ME, Ndoni S, Kristensen A. UV patterned nanoporous solid-liquid core waveguides. Optics Express. 2010;**18**(12):12903-12908

[115] Penadés JS, Ortega-Moñux A, Nedeljkovic M, Wangüemert-Pérez JG, Halir R, Khokhar AZ, Alonso-Ramos C, et al. Suspended silicon mid-infrared waveguide devices with subwavelength grating metamaterial cladding. Optics Express. 2016;**24**(20):22908-22916

[116] Alasaarela T, Saastamoinen T, Hiltunen J, Säynätjoki A, Tervonen A, Stenberg P, Kuittinen M, Honkanen S. Atomic layer deposited titanium dioxide and its application in resonant waveguide grating. Applied Optics. 2010;**49**:4321-4325

[117] Häyrinen M, Roussey M, Gandhi V, Stenberg P, Säynätjoki A, Karvonen L, Kuittinen M, Honkanen S. Low-loss titanium dioxide strip waveguides fabricated by atomic layer deposition. Journal of Lightwave Technology. 2014;**32**(2):208-212

[118] Pandraud G, Barbosa Neira A, Sarro PM, Margallo-Balbás E. PECVD SiC-SiO 2-SiC horizontal slot waveguides for sensing photonics devices. In: Sensors, 2010 IEEE, pp. 975-978. IEEE. 2010

[119] Subramanian AZ, Neutens P, Dhakal A, Jansen R, Claes T, Rottenberg X, Peyskens F, Selvaraja S, Helin P, Du Bois B, et al. Low-loss single mode PECVD silicon nitride photonic wire waveguides for 532–900 nm wavelength window fabricated within a CMOS pilot line. IEEE Photonics Journal. 2013;**5**:2202809-2202809. DOI: 10.1109/JPHOT.2013.2292698

[120] Romero-García S, Merget F, Zhong F, Finkelstein H, Witzens J. Silicon nitride CMOS-compatible platform for integrated photonics applications at visible wavelengths. Optics Express. 2013;**21**:14036-14046

[121] Luke K, Dutt A, Poitras CB, Lipson M. Overcoming Si3N4 film stress limitations for high quality factor ring resonators. Optics Express. 2013;**21**:22829-22833

[122] Bauters JF, Heck MJR, John D, Dai D, Tien M-C, Barton JS, Leinse A, Heideman RG, Blumenthal DJ, Bowers JE. Ultra-low-loss high-aspect-ratio Si 3 N 4 waveguides. Optics Express. 2011;**19**(4):3163-3174

[123] Epping JP, Hoekman M,Mateman R, Leinse A, Heideman RG, van Rees A, van der Slot PJM, Lee CJ, Boller KJ. High confinement, high yield Si3N4 waveguides for nonlinear optical applications. Optics Express. 2015;**23**:642-648

[124] Luke K, Okawachi Y, Lamont MRE, Gaeta AL, Lipson M. Broadband mid-infrared frequency comb generation in a Si3N4 microresonator. Optics Letters. 2015;**40**:4823-4826

[125] Lin PT, Singh V, Kimerling L, Agarwal AM. Planar silicon nitride mid-infrared devices. Applied Physics Letter. 2013;**102**. DOI: 10.1063/1.4812332

[126] Lin PT, Singh V, Lin HYG, Tiwald T, Kimerling LC, Agarwal AM. Low-stress silicon nitride platform for mid-infrared broadband and monolithically integrated microphotonics. Advanced Optical Materials. 2013;**1**:732-739

[127] Belt M, Davenport ML, Bowers JE, Blumenthal DJ. Ultra-low-loss Ta_2O_5-core/SiO_2-clad planar waveguides on Si substrates. Optica. 2017;**4**(5):532-536

[128] Tsuruda K, Fujita M, Nagatsuma T. Extremely low-loss terahertz waveguide based on silicon photonic-crystal slab. Optics Express. 2015;**23**(25):31977-31990

[129] Yang J, Zhao J, Cheng G, Tian H, Lu S, Chen P, Lin L, Liu W. 3D printed low-loss THz waveguide based on Kagome photonic crystal structure. Optics Express. 2016;**24**(20):22454-22460